

Spatio-temporal equilibrium thermodynamics of guided optical waves at positive and negative temperatures

Lucas Zanaglia¹, Josselin Garnier², Claire Michel^{1,3}, Valérie Doya¹,
Mario Ferraro⁴, Stefan Wabnitz⁵, Iacopo Carusotto⁶, Antonio Picozzi⁵

¹ Université Côte d'Azur, CNRS, Institut de Physique de Nice, Nice, France

² CMAP, CNRS, Ecole polytechnique, Institut Polytechnique de Paris, 91120 Palaiseau, France

³ Institut Universitaire de France (IUF), 1 rue Descartes, 75005 Paris, France

⁴ Department of Physics, University of Calabria, Via P. Bucci, Rende, 87036, (CS), Italy

⁵ Department of Information Engineering, Electronics, and Telecommunications,

Sapienza University of Rome, Via Eudossiana 18, Rome, 00184, Italy

⁶ INO-CNR Pitaevskii BEC Center and Dipartimento di Fisica, Università di Trento, 38123 Povo, Italy and

⁷ Université Bourgogne Europe, CNRS, Laboratoire Interdisciplinaire

Carnot de Bourgogne ICB UMR 6303, 21000 Dijon, France

Optical thermalization has been recently studied theoretically and experimentally in the 2D spatial evolution of (quasi-)monochromatic light waves propagating in multimode fibers. In this work, we investigate the spatio-temporal equilibrium properties of incoherent multimode optical waves through the analysis of the (2+1)D Bose-Einstein thermal distribution and the corresponding classical Rayleigh-Jeans approximation. In the anomalous dispersion regime, the spatio-temporal equilibrium is characterized by positive temperatures. In this regime, we show that as the number of modes of the waveguide increases, the fundamental spatial mode becomes macroscopically populated, while its temporal spectrum undergoes significant narrowing, ultimately leading to complete (2+1)D spatio-temporal condensation in the thermodynamic limit. In the normal dispersion regime, the spatio-temporal equilibrium is characterized by negative temperature states that exhibit a hybrid character: the spatial equilibrium displays an inverted modal population, whereas the temporal spectrum remains peaked around the fundamental (carrier) optical frequency. In this regime, we predict that spatio-temporal light waves exhibit a phase transition to Bose-Einstein condensation at negative temperatures, which occurs by increasing the temperature above a negative critical value. Our work opens new avenues for future research, including the possibility for a dual spatio-temporal beam cleaning through full spatio-temporal light condensation, and lay the groundwork for the development of spatio-temporal optical thermodynamics.

I. INTRODUCTION

There is a growing interest in studying quantum fluids of light with effective photon-photon interactions, which may be viewed as the photonic counterpart to atomic Bose gases [1–6]. The concept of fluid of light emerges from a mathematical mapping between the propagation of a light field through a nonlinear medium and the conservative temporal evolution of a quantum fluid of interacting photons [7]. Such propagating fluids of light have been used to explore a wide range of intriguing phenomena, e.g., the generation of superfluid Bogoliubov sound waves [8, 9], complex vortex dynamics [10–14], binary fluids [15], spin-orbit coupled fluids [16, 17], analogue gravity and cosmology [18–23], turbulence cascades regimes [24, 25], or the dynamical formation of prethermalized equilibrium states [26–29].

Among the physical phenomena associated with the propagation of fluids of light, we would like to highlight that full three-dimensional (3D) quantum thermalization and photon condensation have been predicted in a bulk Kerr medium since 2016 [30]. However, because collisional scattering effects are exceedingly rare in the quantum regime, these effects were also anticipated to typically require prohibitively long propagation lengths in standard media. The situation is much different for clas-

sical fields, for which thermalization and condensation are accelerated and eventually made possible in realistic configurations by bosonic stimulation effects [31–36]. Note that these works are to be contrasted to the various forms of non-equilibrium condensation that have been studied in driven-dissipative cavity configurations [2], either in the genuine quantum Bose-Einstein (BE) regime [37–43] or in the classical regime [44–51]. As the steady-state is determined by a dynamical balance of gain and losses, the system does not necessarily tend to a thermal equilibrium condition but may keep displaying peculiar non-equilibrium features [2].

Coming back to propagating geometries described by a conservative evolution, 2D spatial thermalization to the classical Rayleigh-Jeans (RJ) equilibrium distribution has been predicted for optical waves propagating in a multimode fiber [52] on the basis of the wave turbulence theory [35, 36, 53–56]. The finite number of modes of an optical beam in guided configuration accelerates the rate of thermalization to the RJ equilibrium, and also regularizes the ultraviolet catastrophe inherent to classical waves. It is in this guided-wave configuration that RJ thermalization has recently been experimentally studied in the transverse 2D spatial dynamics of a quasi-monochromatic speckle beam that propagates in a multimode fiber [57–62]. This process is associated with the spatial beam self-cleaning effect [63, 64], whose physical

mechanism has been investigated in different theoretical works [56, 65–71], see also the reviews [72, 73]. Furthermore, it has been pointed out that, for higher-order modes, the output mode power distribution that accompanies the beam self-cleaning experiments of [59, 60] can be fitted by the BE law [74], as it was confirmed by experiments in relatively long spans of graded-index (GRIN) multimode fibers [74, 75]. On the other hand, recent experiments indicate that beam-cleaning in a dissipative double-clad fiber can be understood in analogy to BE condensation [76]. From a broader perspective, this intense activity has given rise to the emerging topical area of optical thermodynamics [67, 77–83]. In this context, different important achievements have been obtained, among which we may highlight the prediction [67] and experimental observation of negative temperature equilibrium states [84–86], the calorimetry of photon gases [87], their Joule-Thomson expansion [88], and the development of non-equilibrium thermodynamic approaches [89–93].

The general objective of this article is to lay a groundwork for studying the spatio-temporal (ST) thermodynamic equilibrium properties of guided light waves. This investigation takes inspiration from a number of studies on the coherence properties of an atomic beam evaporatively cooled in a magnetic guide [94–98]. Here, assuming thermal equilibrium in the quantum degenerate regime, it was shown that the atomic beam experiences two-dimensional (2D) transverse BE condensation, rather than a full 3D condensation, because of the very elongated geometry of the magnetic guide [94].

In the optical context, increasing attention is now being devoted to the complex spatio-temporal dynamics of optical beams propagating in multimode fibers, see, e.g., [63, 99–107]. In this respect, we may recall that the turbulent dynamics of purely temporal incoherent optical waves was originally investigated in single mode fibers within the framework of the wave turbulence theory [51, 108–114]. In this framework, temporally incoherent sources – such as amplified spontaneous emission (ASE) – are commonly employed in optical experiments (e.g., [51, 110–112]), which contrasts with the use of coherent laser sources in spatial beam cleaning experiments [72, 73], as it was done in recent investigations into the role of temporal effects in that phenomenon [60, 115–117].

Within the broad context of optical thermalization, we may note that the general form of ST RJ equilibrium distribution [118] has been derived from first principles by considering the conservation laws for optical waves propagating in multimode fibers [61]. In a recent work, the nonequilibrium process of ST thermalization in a multimode waveguide was investigated [119], showing that spatial discrete modes and continuous temporal frequencies cooperate in a joint manner, leading to a significant acceleration of light thermalization towards ST equilibrium.

Specifically, in this work we extend to the (2+1)D case the approach that was recently employed to study purely

spatial 2D equilibrium systems [120], which permits a general understanding of the ST equilibrium properties of multimode guided waves. The analysis reveals different properties depending on the nature of the dispersion regime. In the anomalous dispersion regime we show that, as the waveguide becomes highly multimode, the fundamental mode becomes macroscopically populated while its spectrum undergoes significant spectral narrowing, ultimately leading to a complete (2+1)D spatio-temporal condensation in the thermodynamic limit. On the other hand, in the normal dispersion regime we show that negative temperatures emerge as natural equilibrium states of ST thermalization. These states are characterized by a crossed hybrid nature: in the spatial domain the distribution is inverted, with high-order modes more populated than low-order modes; whereas in the time domain the low-frequency components (relative to the carrier frequency) are more populated than the high-frequency components. In this way, we show that the ST equilibrium distribution undergoes a phase transition to BE condensation at negative temperatures: the highest energy level becomes macroscopically populated at the carrier optical frequency by increasing the optical temperature above a negative critical value.

The article is organized as follows. In Sec. II we introduce the ST equilibrium distributions and characterize their properties for both positive and negative temperatures. Section III focuses on the case of positive temperatures through the analysis of the transition to light condensation in the spatial and ST cases. In doing so, we show that the ST configuration provides a natural distinction between the classical RJ regime and the quantum BE regime. The analysis is extended to negative temperatures in Sec. IV, which is essentially devoted to examining the phase-transition to BE condensation at negative temperatures. Finally, the concluding section discusses possible perspectives and future directions for this work.

II. SPATIO-TEMPORAL EQUILIBRIUM DISTRIBUTION

Let us consider the propagation of a continuous-wave (CW) spatio-temporal incoherent optical field in a multimode waveguide, with temporal fluctuations that are statistically stationary in time, i.e., along the longitudinal waveguide axis. In a previous work [119], a general model of ST propagation in multimode waveguides was introduced, on the basis of the unidirectional propagation equation. This permitted to reveal a fast process of ST thermalization to the equilibrium distribution. Our aim in this article is to derive analytically tractable expressions for the ST thermodynamic equilibrium properties. For this purpose, we consider the minimal ingredients yielding an ST coupling in the framework of a quantum version of the ST nonlinear Schrödinger (NLS) equation, see Ref.[7]. Accordingly, we consider the propagation of

an optical field along the z -axis of a waveguide, which laterally confines the field through a trapping potential $V(\mathbf{r}_\perp)$ set by the refractive index profile in the transverse directions $\mathbf{r}_\perp = (x, y)$. We denote by $n_m(\omega)$ the number of photons at thermal equilibrium in a mode m of the multimode waveguide at frequency ω , which denotes the frequency off-set with respect to the central carrier frequency ω_0 :

$$n_m(\omega) = \frac{1}{\exp\left(\frac{\hbar c_0 \tilde{\beta}_m - \tilde{\mu}}{k_B T}\right) - 1}, \quad (1)$$

where $\tilde{\beta}_m(\omega) = \beta_m - \kappa\omega^2$, with β_m the eigenvalues of the transverse trapping potential $V(\mathbf{r}_\perp)$ (see [121] for relevant examples involving a homogeneous step-index waveguide and a parabolic waveguide). The parameter κ (in s^2/m) is the group-velocity dispersion coefficient, and $c_0 = c/n_{wg}$ the group-velocity at the carrier frequency, n_{wg} being the waveguide (core) refractive index.

In order to make a link with the classical RJ distribution, it proves convenient to introduce the optical temperature $\tilde{T} = k_B T/(\hbar c_0)$ (in m^{-1}), and the optical chemical potential $\tilde{\mu} = \mu/(\hbar c_0)$ (in m^{-1}), which gives

$$n_m(\omega) = \frac{1}{\exp\left(\frac{\tilde{\beta}_m(\omega) - \tilde{\mu}}{\tilde{T}}\right) - 1}, \quad (2)$$

so that the classical wave limit relevant for highly occupied modes $n_m(\omega) \gg 1$, refers to the RJ distribution:

$$n_m^{RJ}(\omega) = \frac{\tilde{T}}{\tilde{\beta}_m(\omega) - \tilde{\mu}}. \quad (3)$$

It is important to recall that the RJ distribution should only be regarded as a formal limit of the BE distribution. Indeed, strictly speaking, the RJ distribution leads to the well-known ultraviolet (UV) catastrophe in the absence of a frequency cut-off along the longitudinal temporal dimension. Although our primary focus in the following will be on the BE distribution, we will keep the RJ limit in mind as a classical approximation, which is valid for the highly populated modes. In addition, it should be noted that the nonequilibrium process of ST thermalization can be characterized by a quasi-equilibrium state that adiabatically follows a local RJ distribution during propagation, as recently discussed in [119]. This shows that the classical RJ distribution also plays a key role in the nonequilibrium route to full ST thermalization.

The physical property $n_m(\omega) > 0$, yields the following conditions on the thermodynamic parameters. If $\kappa < 0$ (anomalous dispersion), temporal dispersion and spatial diffraction operate in the same way, and the equilibrium is characterized by a positive temperature, $\tilde{T} > 0$ with $\tilde{\mu} < \beta_0$. Conversely, if $\kappa > 0$ (normal dispersion), temporal dispersion and spatial diffraction operate in opposite ways, and the equilibrium is characterized by a negative temperature $\tilde{T} < 0$ with $\tilde{\mu} > V_0$, where $V_0 = \max(\beta_m)$ denotes the truncation of the waveguide trapping potential in the transverse spatial dimension. This simple

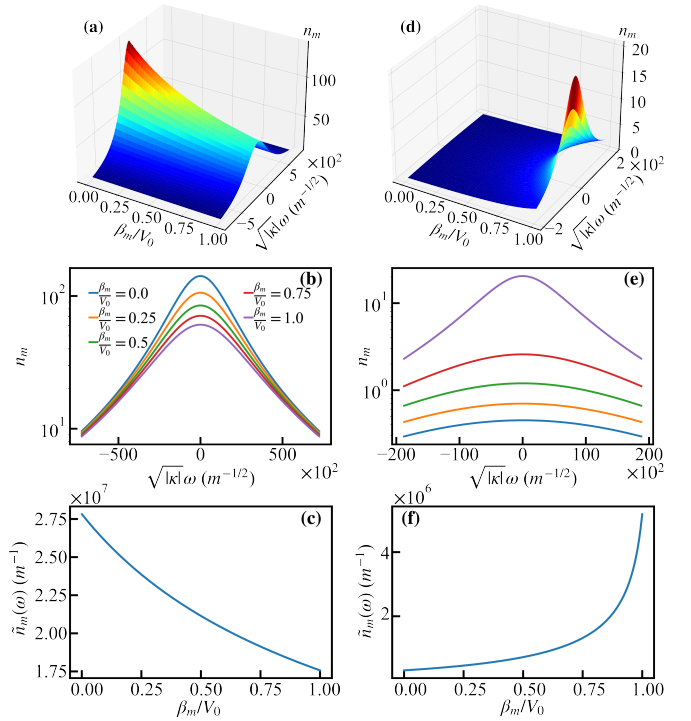


FIG. 1: ST equilibria at positive and negative temperatures. Equilibrium distribution (2) for a step-index multimode waveguide, in the anomalous dispersion regime ($\kappa < 0$) leading to positive temperatures, $\tilde{T} > 0$ (left column), and in the normal dispersion regime ($\kappa > 0$) leading to negative temperatures, $\tilde{T} < 0$ (right column). At variance with $\tilde{T} > 0$ where the spatial and temporal spectra are peaked in the fundamental spatial mode $m = 0$ at frequency $\omega = 0$, for $\tilde{T} < 0$ the equilibrium is featured by an inverted population of spatial modes, with temporal spectra still peaked at $\omega = 0$. The equilibrium distributions are plotted at $\tilde{T} = 1.3\tilde{T}_c$ [left column: (a-b-c)], and $\tilde{T} = -2|\tilde{T}_c|$ [right column: (d-e-f)]. The plots on the first row report the ST distribution $n_m(\omega)$ from Eq.(2), the plots on the second and third rows display cross-sections of the corresponding distributions in the top row: temporal spectra $n_m(\omega)$ for different modes with eigenvalues β_m (2nd row); spatial mode distribution integrated in frequency, $\tilde{n}_m = (2\pi c_0)^{-1} \int n_m(\omega) d\omega$ (3rd row). Parameters are given in the text.

observation shows that negative temperature equilibria emerge as natural equilibrium states of ST thermalization. To summarize, we have:

$$\begin{aligned} \kappa < 0 &\rightarrow \tilde{T} > 0, \tilde{\mu} < \beta_0, \\ \kappa > 0 &\rightarrow \tilde{T} < 0, \tilde{\mu} > V_0. \end{aligned}$$

More precisely, we anticipate that negative temperature ST equilibria are characterized by a crossed hybrid nature: while in the spatial domain the population is inverted (the highest waveguide mode β_{\max} being the most populated), in the temporal domain the fundamental frequency component ($\omega = 0$) is the most populated.

We illustrate the properties of the ST equilibrium BE distribution $n_m(\omega)$ in Fig. 1, for positive and negative temperatures, respectively. In these examples, we have considered circular step-index waveguides with different properties, since the normal and anomalous dispersion regimes typically occur at different wavelengths, which in turn modify the waveguide characteristics and corresponding propagation constants. For instance, this is the case for silica fibers, where the zero-dispersion wavelength is around $\lambda_0 \simeq 1.3\mu\text{m}$ – the dispersion regime being anomalous (normal) for $\lambda > \lambda_0$ ($\lambda < \lambda_0$). It is worth noting that, beyond multimode optical fibers, different alternative waveguide configurations and experimental platforms are available, including, e.g., optically induced waveguides in photorefractive crystals [122] and atomic vapours [29]. In photorefractive SBN crystals, the zero dispersion wavelength is also around $\lambda_0 \simeq 1.3\mu\text{m}$ – dispersion being normal (anomalous) for $\lambda < \lambda_0$ ($\lambda > \lambda_0$) [123]. In atomic vapors, the dispersion can be tuned from positive to negative in the vicinity of an atomic resonance [124], and its magnitude can greatly exceed that encountered in standard optical fibers [4].

A key parameter for the following discussion is the depth of the trapping potential, $V_0 = \pi(n_{wg}^2 - n_0^2)/(\lambda n_{wg})$, where n_{wg} and n_0 are the refractive indices of the waveguide and the surrounding medium, respectively. In the examples shown in Fig. 1, we have considered for $\tilde{T} > 0$ (left column) a step-index waveguide with $V_0 = 52\,726\,m^{-1}$ and a cross-sectional waveguide surface $S = 1.26 \times 10^{-7}\,m^2$, while for $\tilde{T} < 0$ (right column) $V_0 = 126\,093\,m^{-1}$ with $S = 3.14 \times 10^{-8}\,m^2$. In both cases, the optical power is fixed to $P = 1\,\text{W}$, whose relation with the equilibrium distribution $n_m(\omega)$ will be discussed in the next section. Note that, for the particular case of standard silica fibers, the above examples would correspond to $n_{wg} = 1.4516, n_0 = 1.4316$ at $\lambda = 2.4\,\mu\text{m}$ for $\tilde{T} > 0$, and $n_{wg} = 1.4723, n_0 = 1.4623$ at $\lambda = 0.5\,\mu\text{m}$ for $\tilde{T} < 0$.

In Fig. 1(b)-(e), the temporal spectra are plotted as a function of $\sqrt{|\kappa|}\omega$ to show that the typical spectral widths scale as $\sim 1/\sqrt{|\kappa|}$. In this respect, it is important to note that, by an appropriate change of variables [125], the dispersion parameter can be rescaled out of the equilibrium distribution (2), thereby eliminating $|\kappa|$ from all the analysis presented in this work. Consequently, apart from its sign, the exact magnitude of the dispersion parameter $|\kappa|$ has no qualitative impact on the thermodynamic equilibrium properties of the system.

III. POSITIVE TEMPERATURES

A. Spatial analysis in a step-index waveguide

When considering the basic features of BE condensation in low-dimensional systems [126], we may recall that a phase transition to BE (or RJ) condensation can occur

in a 2D parabolic shaped trapping potential, such as a multimode GRIN fiber [120]. Conversely, there is no phase transition (in the thermodynamic limit) to BE or RJ condensation in a 2D homogeneous step-index waveguide. In other terms, in the purely 2D spatial case, the observation of a macroscopic population of the fundamental mode in a step-index waveguide would only be a finite size effect, which would eventually disappear by increasing the system size (see, e.g., Fig. 5 in [120]). In the following, we address the issue of light condensation in a step-index waveguide in the (2+1)D ST configuration.

As mentioned in the introduction, this problem was considered by studying the coherence properties of an atom laser beam in a magnetic guide [94], where it was shown that the atomic beam does not undergo a full three-dimensional BE condensation. Indeed, because of the highly elongated geometry of the considered magnetic guide, the system was shown to exhibit a macroscopic population of the fundamental mode in the transverse 2D spatial dimensions, while preserving long-wavelength fluctuation that destroy long-range order in the longitudinal direction – full condensation was recovered in the limit of a shallow transverse confinement. This was a consequence of the anisotropic spatial constraints imposed by the magnetic confinement, which significantly altered the condensation behavior of the atomic ensemble. Here, we revisit this problem in the context of multimode optical waveguides, where the transverse waveguide supports a finite number of spatial modes, i.e., the potential that confines the optical field in the transverse spatial dimension is truncated, $V_0 < \infty$. We first study the thermal equilibrium properties of the transverse spatial mode distribution, and then show that, by increasing the number of spatial modes M , the temporal spectrum exhibits significant narrowing, until full (2+1)D ST condensation is achieved in the thermodynamic limit.

1. Finite number of spatial modes

Let us recall that we consider a continuous temporal incoherent optical wave, characterized by fluctuations that are statistically stationary in time. Then the relevant quantity for characterizing the field is not the number of photons N , but the longitudinal density of photons, $\rho = N/L$ (in m^{-1}). Following [30], the longitudinal photon density takes the form:

$$\rho = \sum_{m=0}^{M-1} \int \frac{d\omega}{2\pi c_0} \frac{1}{e^{(\beta_m + |\kappa|\omega^2 - \tilde{\mu})/\tilde{T}} - 1} \quad (4)$$

$$= \frac{\sqrt{\pi}}{2\pi c_0} \sqrt{\frac{\tilde{T}}{|\kappa|}} \sum_{m=0}^{M-1} g_{1/2} \left(e^{(\tilde{\mu} - \beta_m)/\tilde{T}} \right) \quad (5)$$

where $g_p(z) = \frac{1}{\Gamma(p)} \int_0^\infty dx \frac{x^{p-1}}{z^{-1} e^x - 1} = \sum_{l=1}^\infty \frac{z^l}{l^p}$ is the Bose function, and $\zeta(p) = g_p(1)$ is the Riemann function [126]. In other terms, in (5) we have considered the continuous

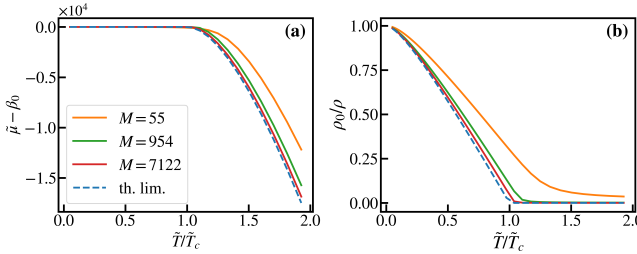


FIG. 2: Condensation at positive temperatures. Convergence to the thermodynamic limit for $\tilde{T} > 0$ in a step-index waveguide: (a) chemical potential vs temperature, $\tilde{\mu}(\tilde{T})$; (b) spatial condensate fraction vs temperature, $\rho_0(\tilde{T})/\rho$. The solid lines refer to the computation of the discrete sums beyond the thermodynamic limit, from Eq.(5) for (a), and from Eq.(6) for (b). By increasing the number of modes M (or the waveguide surface S) while keeping the photon density $\rho/S = \text{const}$ and $V_0 = \text{const}$, the curves approach the thermodynamic limit (dashed blue line), which are obtained from Eq.(8) for (a), and from Eq.(10) for (b). In the thermodynamic limit, $\tilde{\mu}(\tilde{T})$ in (a), and $\rho_0(\tilde{T})/\rho$ in (b), correspond to the (2+1)D ST condensation: both curves display a singular cusped behavior at $\tilde{T} = \tilde{T}_c$, where $\tilde{\mu} = \beta_0$ for $0 < \tilde{T} \leq \tilde{T}_c$, and $\rho_0 = 0$ for $\tilde{T} > \tilde{T}_c$, where the critical temperature \tilde{T}_c is given by Eq.(9). Parameters are given in the text.

(thermodynamic) limit in the time domain, because there is no confinement along the temporal dimension; whereas we keep a discrete sum over the transverse spatial modes of the waveguide. We recall that we are considering in this section the anomalous dispersion regime for positive temperatures, $\tilde{T} > 0$ and $\kappa < 0$ in Eqs.(4-5).

Denoting by ρ_0 the photon density in the fundamental spatial mode $m = 0$ (i.e., integrated along the frequency ω), the fraction of photon density that populates the fundamental transverse mode is

$$\frac{\rho_0}{\rho} = 1 - \frac{\sqrt{\pi}}{2\pi c_0 \rho} \sqrt{\frac{\tilde{T}}{|\kappa|}} \sum_{m \neq 0}^{M-1} g_{1/2} \left(e^{(\tilde{\mu} - \beta_m)/\tilde{T}} \right). \quad (6)$$

Consequently, ρ_0/ρ can be viewed, in a loose sense, as the ‘spatial condensate’ fraction of the ST system for a finite transverse size of the waveguide, i.e., for finite number of modes M .

2. Toward the continuous thermodynamic limit

In the following, we consider highly multimode waveguides, and extend the procedure described in [120] for the pure 2D spatial case to the ST (2+1)D problem under consideration. More precisely, we study how the system approaches the thermodynamic limit, that is the limit where the waveguide surface tends to infinity $S \rightarrow \infty$, while keeping constant the three-dimensional photon density $\rho/S = N/(SL) = \text{const}$ (in m^{-3}) and the potential depth, $V_0 = \text{const}$ [120]. Note that the photon density ρ/S is proportional to the optical intensity

$I = P/S$, where P is the beam power (in W), because $\rho = P/(c_0 \hbar \omega_0)$. In this way, for a given beam intensity I (or equivalently ρ/S), Eq.(5) provides a closed relation between the chemical potential and the temperature $\tilde{\mu}(\tilde{T})$, which is reported in Fig. 2 for different values of S (i.e., different number of modes M). As evidenced in Fig. 2, as the system size S increases (or equivalently M increases), the curves $\tilde{\mu}(\tilde{T})$ converge to the continuous limit (dashed blue line), where the chemical potential reaches the fundamental eigenvalue $\tilde{\mu} = \beta_0$, below a certain critical temperature \tilde{T}_c (which will be defined below). In the example of Fig. 2, we considered a step-index waveguide with $V_0 = 52726 \text{ m}^{-1}$, $\kappa = -5.3 \times 10^{-24} \text{ s}^2 \cdot \text{m}^{-1}$, while the number of modes M (or the surface S) is increased by keeping constant the three-dimensional photon density $\rho/S = 2.07 \times 10^{16} \text{ m}^{-3}$ (or intensity $I = P/S = 3.54 \times 10^5 \text{ W} \cdot \text{m}^{-2}$).

Analyzing the thermodynamic limit is essential. It is in this limit that phase transitions are usually recognized and characterized by a singular (discontinuous) behavior of the thermodynamic quantities when the control parameter (e.g., the temperature) is varied across the transition point. In addition, the advantage of the continuous limit is that it enables us to derive thermodynamic relations in explicit analytical form. In the continuous approach, the discrete sum over the spatial modes can be converted to continuous integrals

$$\sum_{m=0}^{M-1} \rightarrow \int_0^{V_0} d\beta \varrho(\beta), \quad (7)$$

where $\varrho(\beta)$ is the density of states (DOS) [126]. The continuous approach is justified when the equilibrium distribution populates a large number of modes, that is, the optical temperature is much higher than the typical spacing between mode eigenvalues $\tilde{T} \gg \delta\beta$ [126]. We recall that, as commented above through Eqs.(4-5), we have considered the continuous thermodynamic limit in the temporal dimension, along which there is no confinement.

Referring to the step-index waveguide under consideration in Fig. 2, the DOS does not depend on the propagation constant, $\varrho(\beta) = \varrho_0 = k_0 S/(2\pi)$, with $k_0 = 2\pi n_{wg}/\lambda$, as typical for 2D systems with no confinement potential. In the continuous thermodynamic limit, the longitudinal photon density is obtained from Eq.(5) by converting the discrete sum over the transverse m modes into a continuous integral [see (7)], which gives

$$\rho = \frac{\varrho_0 \sqrt{\pi}}{2\pi c_0} \frac{\tilde{T}^{3/2}}{\sqrt{|\kappa|}} \left[g_{3/2}(z) - g_{3/2}(ze^{-V_0/\tilde{T}}) \right], \quad (8)$$

where $z = e^{(\tilde{\mu} - \beta_0)/\tilde{T}}$ is the fugacity. Note that the second term in the square brackets in (8) is specific to our waveguide geometry featured by a truncated potential, $V_0 < \infty$. The analysis of Eq.(8) reveals that, by decreasing the temperature, the chemical potential reaches the fundamental mode eigenvalue, $\tilde{\mu} \rightarrow \beta_0^-$ (i.e., $z \rightarrow 1^-$) for a non-vanishing critical temperature $\tilde{T}_c > 0$, which is

solution of

$$\rho = \frac{\rho_0 \sqrt{\pi}}{2\pi c_0} \frac{\tilde{T}_c^{3/2}}{\sqrt{|\kappa|}} \left[\zeta(3/2) - g_{3/2}(e^{-V_0/\tilde{T}_c}) \right]. \quad (9)$$

For lower temperatures $T < \tilde{T}_c$, a macroscopic fraction ρ_0/ρ of the density is concentrated in the $m = 0$ transverse mode [94]. A plot of the chemical potential vs temperature is reported in Fig. 2(a): as the number of modes increases, the curves tend to the thermodynamic limit curve indicated by the dashed blue line.

An explicit formula for the spatial condensate fraction for $\tilde{T} \leq \tilde{T}_c$ can be obtained by considering Eq.(6) in the continuous limit and setting $\tilde{\mu} = \beta_0$,

$$\frac{\rho_0}{\rho} = 1 - \left(\frac{\tilde{T}}{\tilde{T}_c} \right)^{3/2} \frac{\zeta(3/2) - g_{3/2}(e^{-V_0/\tilde{T}})}{\zeta(3/2) - g_{3/2}(e^{-V_0/\tilde{T}_c})}. \quad (10)$$

A plot of the spatial condensate fraction is reported in Fig. 2(b): once again, as the number M of modes increases, the curve tends to the thermodynamic limit result (10) indicated by the dashed blue line.

B. ST condensation in a step-index waveguide

Let us now analyze the phase transition to full ST condensation in the lowest $\omega = 0$ state of the fundamental mode $m = 0$. We follow the usual treatment of BE condensation in the thermodynamic limit [126]. For $\tilde{T} < \tilde{T}_c$, we split the contribution of the singularity of the BE distribution at $\omega = 0$ and $m = 0$, and the thermal contribution $\rho = \rho_{00} + \int_0^{V_0} d\beta \varrho_0 \int \frac{d\omega}{2\pi c_0} (e^{(\beta+|\kappa|\omega^2)/\tilde{T}} - 1)^{-1}$ in all other states.

According to the standard theory of BE condensation [126], the photon gas then undergoes a phase transition to ST condensation, characterized by a macroscopic population of the $\omega = 0$ state of the fundamental spatial mode $m = 0$,

$$\frac{\rho_{00}}{\rho} = 1 - \left(\frac{\tilde{T}}{\tilde{T}_c} \right)^{3/2} \frac{\zeta(3/2) - g_{3/2}(e^{-V_0/\tilde{T}})}{\zeta(3/2) - g_{3/2}(e^{-V_0/\tilde{T}_c})}, \quad (11)$$

where the critical temperature \tilde{T}_c is still given by Eq.(9). Accordingly, the ST condensate fraction ρ_{00}/ρ vanishes for $\tilde{T} > \tilde{T}_c$, while it increases to 1 when the temperature decreases below \tilde{T}_c and tends to 0.

It is important to stress that, in the thermodynamic limit, the condensate fraction for the spatial case in Eq.(10), and the ST case in Eq.(11), are identical: the total population ρ_0 in the fundamental spatial mode $m = 0$ (i.e., integrated along the frequency ω) is in fact dominated by the population ρ_{00} of the fundamental mode $m = 0$ at $\omega = 0$, while the contribution to the photon density at $m = 0$ provided by the $\omega \neq 0$ states is negligible. This is expected in the continuous approximation in the ST domain. Indeed, the expression (1)

shows that only $m = 0$, $\omega = 0$ may present a singularity. Therefore, in the continuous approximation in the ST domain the photon distribution presents a singular (Dirac- δ) contribution at $\beta = 0$, $\omega = 0$ with weight ρ_{00} and a continuous contribution with density with respect to the 2D Lebesgue measure in β and ω and with total weight $\rho - \rho_{00}$. We remind the reader that the 2D Lebesgue measure of a line is zero and that any measure that has a density with respect to the 2D Lebesgue measure satisfies the same property (because any measure that admits a density with respect to the 2D Lebesgue measure automatically assigns measure zero to any set that has 2D Lebesgue measure zero). Thus, the integral with respect to ω at $\beta = 0$ (that gives ρ_0) is equal to the weight ρ_{00} of the singular contribution at $\beta = 0$, $\omega = 0$.

We finally remark that Eq.(8) encompasses the standard criterion for BE condensation of a dilute 3D Bose gas in the thermodynamic limit [126]. Indeed, in the absence of a cut-off waveguide ($V_0 \rightarrow \infty$), we can follow [30] by introducing the thermal wavelengths in the transverse and longitudinal dimensions, $\lambda_{\perp,\parallel} = (2\pi\hbar^2/(m_{\perp,\parallel} k_B T))^{1/2} = (4\pi\alpha_{\perp,\parallel}/\tilde{T})^{1/2}$, with the effective masses $m_{\perp} = \hbar k_0/c_0$, $m_{\parallel} = \hbar/(2c_0^3|\kappa|)$, and corresponding spatial (diffraction) and temporal (dispersion) coefficients, $\alpha_{\perp} = 1/(2k_0)$ and $\alpha_{\parallel} = \kappa c_0^2$, respectively. In this way, Eq.(8) can be written at $\tilde{T} = \tilde{T}_c$ in the form $\lambda_{\parallel} \lambda_{\perp}^2 \rho/S = \zeta(3/2)$. This expression recovers the standard criterion for BE condensation in 3D: condensation arises at $\lambda_{\parallel} \lambda_{\perp}^2 \rho/S \sim 1$, which can be reached either by increasing the photon density ρ/S , or by decreasing the temperature \tilde{T} , i.e., by increasing the thermal wavelengths.

C. Spectral narrowing by increasing the number of modes

We have seen that 2D spatial condensation tends to evolve into full (2+1)D ST condensation by increasing the transverse surface size of the waveguide. This suggests that the temporal spectrum of the fundamental mode should exhibit significant spectral narrowing as the waveguide becomes wider. We illustrate this remarkable property in Fig. 3, which reports the ST equilibrium distribution $n_m(\omega)$ given in Eq.(2) for a small waveguide ($M = 17$ modes, left column), and a large waveguide ($M = 954$ modes, right column). In this figure, we have considered a partially condensed case where $\tilde{T} = 0.6\tilde{T}_c$. Note that although $\tilde{T} < \tilde{T}_c$, we have $\tilde{\mu} \neq \beta_0$, because the waveguides have a finite size and the system is not in the thermodynamic limit. Accordingly, the value of the chemical potential $\tilde{\mu}$ is obtained by solving Eq.(5). In the example of Fig. 3 we have considered the following parameters: $\rho/S = 2.1 \times 10^{16} m^{-3}$, $P = 0.1 W$, $V_0 = 52725 m^{-1}$, with waveguide radius $R = 14 \mu m$ for $M = 17$, and $R = 100 \mu m$ for $M = 954$.

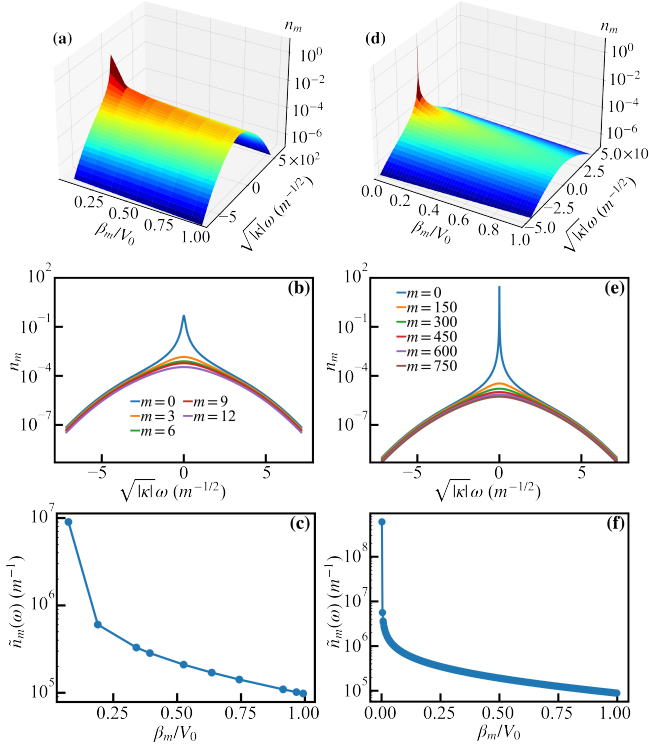


FIG. 3: Spatial mode distribution and temporal spectra in the condensed regime at positive temperatures. Equilibrium distribution (2) for a step-index waveguide at $\tilde{T} = 0.6\tilde{T}_c$ for $M = 17$ [left column: (a-b-c)], and $M = 954$ [right column: (d-e-f)]. The plots on the first row report the ST distribution $n_m(\omega)$ from Eq.(2), the plots on the second and third rows display cross-sections of the corresponding distributions in the top row: temporal spectra $n_m(\omega)$ for different modes m (2nd row); spatial mode distribution integrated in frequency, $\tilde{n}_m = (2\pi c_0)^{-1} \int n_m(\omega) d\omega$ (3rd row). By increasing the number of modes M , we observe a significant spectral narrowing of the fundamental mode (compare (b) and (e)), as well as a macroscopic population of the fundamental spatial mode $m = 0$ (compare (c) and (f)). Parameters are given in the text.

The comparison of Fig. 3(b) and Fig. 3(e) reveals the occurrence of a significant spectral narrowing of the fundamental mode as the waveguide size (or number of modes M) increases. At the same time, the fundamental spatial mode gets macroscopically populated, as can be seen by the comparison of Fig. 3(c) and Fig. 3(f).

D. BE vs RJ regimes

The BE distribution is known to recover the classical RJ distribution in the limit of highly occupied modes. However, discussing the RJ regime is not straightforward because, as noted above, the RJ distribution leads to the well-known UV catastrophe (signalled, e.g., by a divergence of the energy density [127]) in the absence of a high-frequency cut-off. Nonetheless, it is worth noting that the one-dimensional integral over temporal frequen-

cies appearing in the expression of the photon density (4) remains convergent for the RJ law. Based on this observation, we proceed to assess the validity of the RJ approximation by formally substituting the BE law with the RJ law, while keeping in mind that the RJ regime is prone to UV divergences in the ST context.

Estimating the number of photons N in usual beam-cleaning experiments using optical pulses with a finite temporal duration is not immediate, because $N \simeq P\tau/(\hbar\omega_0)$ depends on the temporal duration τ of the (quasi-)monochromatic optical pulse. This would lead to the inconsistent conclusion that an experiment performed with a CW laser beam would involve an infinite number of photons. As previously mentioned, the natural relevant parameter to study (2+1)D ST thermalization is not the total number of photons, but the longitudinal photon density ρ .

We illustrate this in Fig. 4(a), which reports the transition from the BE to the RJ regime by increasing the optical power, which is related to the photon density by $\rho = P/(c_0\hbar\omega_0)$, as previously discussed. In this example, we considered a parabolic waveguide (with radius $R = 300\mu\text{m}$, $V_0 = 52.726\text{m}^{-1}$, $\kappa = -5.3 \times 10^{-24}\text{s}^2 \cdot \text{m}^{-1}$). The DOS for a truncated parabolic waveguide is $\varrho(\beta) = \beta/\beta_0^2$ for $\beta \leq V_0$, and $\varrho(\beta) = 0$ for $\beta > V_0$ [52, 120]. Accordingly, the photon density in the continuous limit at $\tilde{T} = \tilde{T}_c$ reads

$$\rho = \frac{1}{2c_0\beta_0^2} \frac{\tilde{T}_c^{5/2}}{\sqrt{\pi|\kappa|}} \left[\zeta\left(\frac{5}{2}\right) - g_{5/2}\left(e^{-\frac{V_0}{\tilde{T}_c}}\right) - \frac{V_0}{\tilde{T}_c} g_{3/2}\left(e^{-\frac{V_0}{\tilde{T}_c}}\right) \right]. \quad (12)$$

For large powers, all modes are highly occupied, and the photon density is well approximated by the RJ limit $\rho^{RJ} = \frac{V_0^{3/2}}{3c_0\beta_0^2\sqrt{|\kappa|}}\tilde{T}_c$, see the dashed-orange line in Fig. 4(a). By decreasing the power, quantum effects associated to the exponential decay of the BE distribution at high energy play a role, and the photon density follows the behavior $\rho \simeq \frac{\zeta(5/2)}{2c_0\beta_0^2\sqrt{\pi|\kappa|}}\tilde{T}_c^{5/2}$, which is obtained from Eq.(12) without spatial frequency cutoff ($V_0 \rightarrow \infty$), see the dashed green line in Fig. 4(a). More precisely, in the example of Fig. 4, we considered a parabolic waveguide with $G = 94$ groups of degenerate modes, where the number of guided modes is $M = G(G+1)/2 \simeq G^2/2$ for $G \gg 1$.

1. Spatial mode distribution and temporal spectra

The validity of the RJ approximation can be assessed through the analysis of the spatial mode distribution $\tilde{\rho}_S(\beta)$, and the temporal spectrum $\tilde{\rho}_T(\omega)$ of the field,

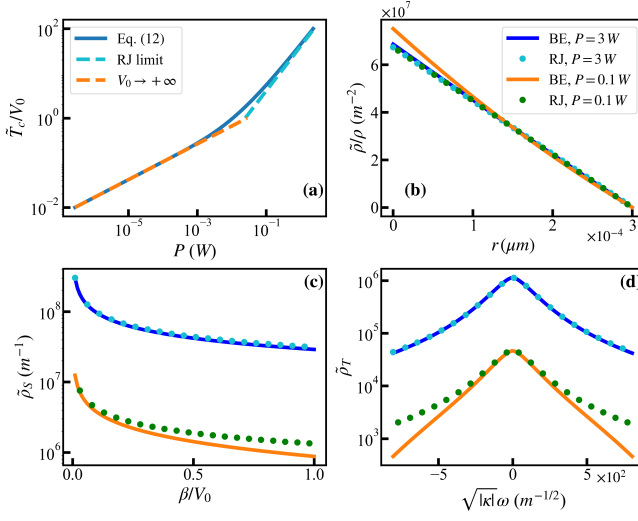


FIG. 4: BE vs RJ regimes. Relation between the optical power P and the critical temperature \tilde{T}_c to condensation, from Eq.(12) (blue line), for a parabolic multimode waveguide. For large powers $P \gg 0.1$ W, the photon density can be approximated by the RJ limit (dashed orange line, $\tilde{T}_c \sim P$). By decreasing the power, the photon density follows the BE expression (12) with $V_0 \rightarrow \infty$ (dashed green line, $\tilde{T}_c \sim P^{2/5}$). Transverse 2D intensity distribution $\tilde{\rho}(r)$ (with $r = |\mathbf{r}_\perp|$) (b), spatial mode distribution $\tilde{\rho}_S(\beta)$ (c), and temporal spectrum $\tilde{\rho}_T(\omega)$ (d), computed with the BE law (solid lines), and the corresponding RJ approximation (dotted lines), at $\tilde{T} = \tilde{T}_c$. As seen in panels (b) to (d), at large power ($P = 3$ W), the distributions are well approximated by the RJ law, while at small power ($P = 0.1$ W) noticeable deviations emerge. Parameters are given in the text.

defined as the two marginal distributions of $n(\beta, \omega)$,

$$\tilde{\rho}_S(\beta) = \int \frac{d\omega}{2\pi c_0} n(\beta, \omega), \quad (13)$$

$$\tilde{\rho}_T(\omega) = \int_0^{V_0} d\beta \varrho(\beta) n(\beta, \omega). \quad (14)$$

We report in Fig. 4(c)-(d) plots of such marginal distributions at $\tilde{T} = \tilde{T}_c$, which are computed with the BE law $n(\beta, \omega) = (e^{(\beta+|\kappa|\omega^2)/\tilde{T}_c} - 1)^{-1}$ (solid lines), and the corresponding RJ approximation $n^{RJ}(\beta, \omega) = \tilde{T}_c/(\beta+|\kappa|\omega^2)$ (dotted lines). We note in panels (c)-(d) of Fig. 4 that for high power, the distributions closely follow the RJ approximation, whereas for low powers a clear deviation is observed.

2. Spatial intensity distribution

The measurement of the modal distribution in an optical fiber experiment is known to be quite complicated, see, e.g., [59, 60, 107, 128]. Here, we discuss another important quantity that is experimentally accessible and that can be exploited to discriminate between the classi-

cal and quantum regimes. This quantity refers to the spatial intensity distribution of the optical field in the transverse spatial dimension \mathbf{r}_\perp . It can be calculated from the semi-classical approximation by writing the equilibrium distribution in the form [126]:

$$n(\mathbf{k}_\perp, \mathbf{r}_\perp, \omega) = \left(e^{\frac{\alpha_\perp k_\perp^2 + |\kappa|\omega^2 + V(\mathbf{r}_\perp) - \tilde{\mu}}{\tilde{T}}} - 1 \right)^{-1}, \quad (15)$$

where $V(\mathbf{r}_\perp)$ is the waveguide trapping potential in the transverse dimension, \mathbf{k}_\perp the corresponding wave-vector, and recall that $\alpha_\perp = 1/(2k_0)$ is the diffraction coefficient. The spatial density distribution is obtained by integration in both spatial and temporal frequency space, which gives

$$\begin{aligned} \tilde{\rho}(\mathbf{r}_\perp) &= \int \frac{d^2 \mathbf{k}_\perp}{(2\pi)^2} \int \frac{d\omega}{2\pi c_0} n(\mathbf{k}_\perp, \mathbf{r}_\perp, \omega) \\ &= \frac{1}{8\pi^{3/2} c_0} \frac{\tilde{T}^{3/2}}{\alpha_\perp \sqrt{|\kappa|}} \left[g_{3/2} \left(e^{-\frac{V(\mathbf{r}_\perp) - \tilde{\mu}}{\tilde{T}}} \right) \right. \\ &\quad \left. - g_{3/2} \left(e^{-\frac{V_0 - \tilde{\mu}}{\tilde{T}}} \right) \right]. \end{aligned} \quad (16)$$

The corresponding intensity distribution in the RJ approximation reads $\tilde{\rho}^{RJ}(\mathbf{r}_\perp) = \frac{\tilde{T}}{4\pi c_0 \alpha_\perp \sqrt{|\kappa|}} (\sqrt{V_0 - \tilde{\mu}} - \sqrt{V(\mathbf{r}_\perp) - \tilde{\mu}})$, which is obtained from $n^{RJ}(\mathbf{k}_\perp, \mathbf{r}_\perp, \omega) = \tilde{T}/(\alpha_\perp k_\perp^2 + |\kappa|\omega^2 + V(\mathbf{r}_\perp) - \tilde{\mu})$. Considering the example of a parabolic waveguide, we report in Fig. 4(b) the intensity distribution (solid lines), and the corresponding RJ approximation (dotted lines), at $\tilde{T} = \tilde{T}_c$. As for panels (c)-(d), a good agreement is obtained with the RJ approximation at high power. Conversely, at low power a pronounced, cusp-like deviation from the RJ distribution appears near the center of the trapping potential.

We finally note that, by integrating the density distribution $\tilde{\rho}(\mathbf{r}_\perp)$ in the 2D transverse spatial domain over $|\mathbf{r}_\perp| \leq R$ (R being the waveguide radius with $V(|\mathbf{r}_\perp| = R) = V_0$), we recover the total density of photons discussed above in the continuous limit

$$\rho = \int_{|\mathbf{r}_\perp| \leq R} \tilde{\rho}(\mathbf{r}_\perp) d\mathbf{r}_\perp = \int \frac{d\omega}{2\pi c_0} \int_0^{V_0} d\beta \varrho(\beta) n(\beta, \omega). \quad (17)$$

IV. BOSE-EINSTEIN CONDENSATION AT NEGATIVE TEMPERATURES

The idea of negative temperatures was originally proposed in the seminal works by Onsager [129] and Ramsey [130]. Significant efforts have been devoted to the theoretical understanding of these unusual thermodynamic equilibrium states. The concept of negative temperatures is now broadly accepted, as it has been the subject of different experimental observations [131–137]. As a matter of fact, negative temperatures were originally experimentally observed in the context of nuclear

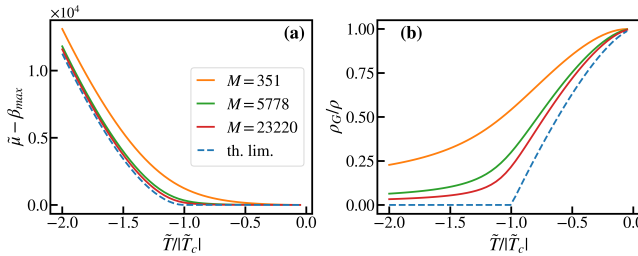


FIG. 5: Condensation at negative temperatures. Convergence to the thermodynamic limit for $\tilde{T} < 0$ in a parabolic waveguide: (a) chemical potential vs temperature, $\tilde{\mu}(\tilde{T})$; (b) condensate fraction in the highest mode group vs temperature, $\rho_G(\tilde{T})/\rho$. The solid lines refer to the computation of the discrete sums beyond the thermodynamic limit, from Eq.(18) (a), and from Eq.(19) (b). By increasing the number of modes M (or the waveguide surface S) while keeping the photon density $\rho/S = \text{const}$ and $V_0 = \text{const}$, the curves approach the thermodynamic limit (dashed blue lines), which are obtained from Eq.(24) for (a), and from Eq.(22) for (b). In the thermodynamic limit, $\tilde{\mu}(\tilde{T})$ in (a), and $\rho_G(\tilde{T})/\rho$ in (b), correspond to the (2+1)D ST condensation: both curves display a singular cusped behavior at $\tilde{T} = \tilde{T}_c < 0$, where $\tilde{\mu} = \beta_{\max} = V_0$ for $\tilde{T}_c \leq \tilde{T} \leq 0$, and $\rho_G = 0$ for $\tilde{T} < \tilde{T}_c < 0$. Parameters are given in the text.

spin systems [138], and more recently with cold atoms in optical lattices [139], and in 2D quantum superfluids [140, 141]. More recently, negative temperatures have been predicted for classical multimode optical wave systems in Ref. [67], and subsequently observed in these systems with light waves in Refs. [84–86]. In particular, in the experiments reported in Ref.[86], negative temperatures were associated to the strongly nonlinear regime of a dense photon gas.

As anticipated above, negative temperatures emerge as natural equilibrium states in ST thermalization, whenever one considers the normal dispersion regime, see Fig. 1. We will now show that negative temperature ST equilibrium states exhibit a phase transition to BE condensation at $\beta = \beta_{\max}$ and $\omega = 0$. We recall that in the purely 2D spatial domain, BE condensation at negative temperatures does not exist, as discussed in [120].

A. Spatial analysis

ST condensation at negative temperatures can take place in a parabolic multimode waveguide or in a homogeneous step-index waveguide, as discussed in the Appendix VII. In the following, we consider the case of a parabolic waveguide (e.g., GRIN multimode fiber), because the highest energy level is highly degenerate, which makes the transition to BE condensation of a different nature with respect to conventional condensation in the (non-degenerate) fundamental mode for $\tilde{T} > 0$. We recall

that the mode eigenvalues read $\beta_m = \beta_0(m_x + m_y + 1)$, where $m = (m_x, m_y)$ labels the two integers that specify a mode [121], and that the waveguide supports G groups of degenerate modes, with $M \simeq G^2/2$ the number of modes ($G \gg 1$).

Considering the normal dispersion regime $\kappa > 0$ ($\tilde{T} < 0$ and $\tilde{\mu} > V_0$), the photon density integrated along the frequency ω reads

$$\rho = \frac{\sqrt{\pi}}{2\pi c_0} \sqrt{\frac{-\tilde{T}}{\kappa}} \sum_m g_{1/2} \left(e^{(\beta_m - \tilde{\mu})/(-\tilde{T})} \right). \quad (18)$$

Denoting by ρ_G the photon density that populates the highest transverse modes with eigenvalue $\beta = \beta_{\max} = V_0$, we have

$$\frac{\rho_G}{\rho} = 1 - \frac{\sqrt{\pi}}{2\pi c_0 \rho} \sqrt{\frac{-\tilde{T}}{\kappa}} \sum_m' g_{1/2} \left(e^{(\beta_m - \tilde{\mu})/(-\tilde{T})} \right), \quad (19)$$

where \sum_m' denotes a sum over all modes except the highest mode group β_{\max} .

We now study how the system approaches the thermodynamic limit by following the procedure of section III A. By keeping fixed the beam intensity $I = P/S$ (or equivalently the photon density $\rho/S = \text{const}$), Eq.(18) provides a closed relation between $\tilde{\mu}$ and \tilde{T} , which is reported in Fig. 5 for different values of the surface S (i.e., different G), while keeping constant ρ/S and V_0 . Note that the waveguide surface is $S = \pi R^2$, where we recall that the waveguide radius is defined by $V(|\mathbf{r}_\perp| = R) = V_0$. Consequently, the surface scales as $S \sim V_0/\beta_0^2$, and the thermodynamic limit for the parabolic waveguide is taken by keeping fixed $\rho\beta_0^2 = \text{const}$ and $V_0 = \text{const}$. In the example of Fig. 5, we considered a parabolic waveguide with $V_0 = 126\,093\,m^{-1}$, $\kappa = 3.6 \times 10^{-25}\,s^2 \cdot m^{-1}$, with $\rho/S = 4.4 \times 10^{16}\,m^{-3}$ (or $I = P/S = 3.5 \times 10^6\,W \cdot m^{-2}$). We note in Fig. 5(a) that, as the transverse waveguide surface S increases, the curves $\tilde{\mu}(\tilde{T})$ converge to the continuous limit, which will be discussed in the next section.

B. ST condensation in the highest energy level

Following the analysis of section III, the spatial condensate fraction of the photon density (19) converges to the ST condensate fraction by increasing the size of the waveguide toward the thermodynamic limit. We now analyze the phase transition to ST condensation in the highest mode group β_{\max} at $\omega = 0$. In a way akin to the case of positive temperatures, condensation at negative temperatures originates in the singularity of the BE equilibrium distribution. By increasing the negative temperature, the chemical potential decreases, and reaches the highest energy level $\tilde{\mu} = \beta_{\max} = V_0$ at a non-vanishing negative critical temperature, $\tilde{T}_c < 0$ (see Fig. 5(a)). Considering the continuous limit, the longitudinal photon density reads $\rho = \int \frac{d\omega}{2\pi c_0} \int_0^{V_0} d\beta \varrho(\beta) n(\beta, \omega)$,

where we recall that the DOS for a parabolic waveguide is given by $\varrho(\beta) = \beta/\beta_0^2$ for $\beta \leq V_0$, and $\varrho(\beta) = 0$ for $\beta > V_0$. At the critical temperature $\tilde{T} = \tilde{T}_c$, we set $\tilde{\mu} = V_0$, and the integration over β gives

$$\rho = \frac{V_0^2}{2\pi c_0 \beta_0^2} \int_{-\infty}^{\infty} d\omega \left[\frac{\tilde{T}_c}{V_0} \ln \left(1 - e^{\frac{\kappa\omega^2}{\tilde{T}_c}} \right) - \frac{\tilde{T}_c^2}{V_0^2} g_2 \left(e^{\frac{\kappa\omega^2}{\tilde{T}_c}} \right) \right. \\ \left. + \frac{\tilde{T}_c^2}{V_0^2} g_2 \left(e^{\frac{\kappa\omega^2 + V_0}{\tilde{T}_c}} \right) \right]. \quad (20)$$

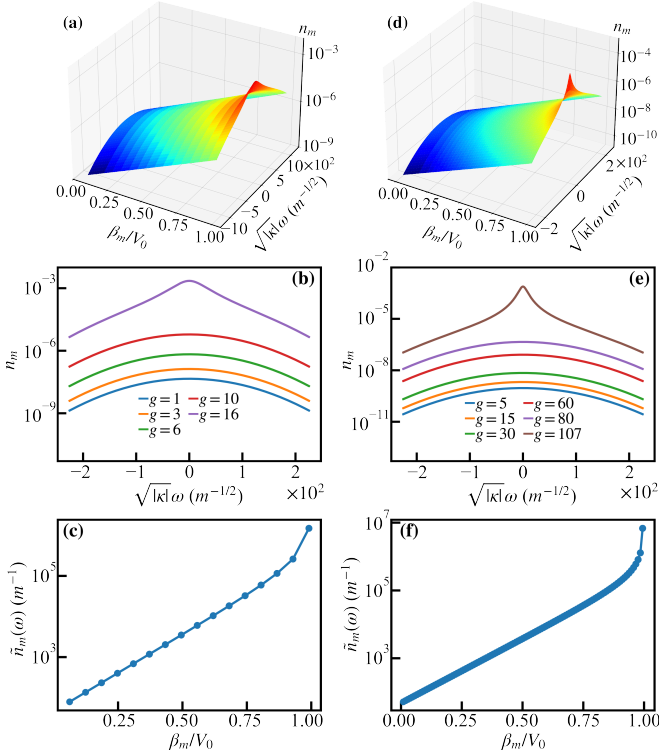


FIG. 6: **Spatial mode distribution and temporal spectra in the condensed regime at negative temperatures.** Equilibrium distribution (2) for a parabolic multimode waveguide (e.g., GRIN multimode fiber) in the normal dispersion regime ($\kappa > 0$) leading to negative temperatures $\tilde{T} = -0.4|\tilde{T}_c|$: for $G = 16$ groups of degenerate modes ($M = 136$ modes) see the left column, and for $G = 107$ groups of degenerate modes ($M = 5778$ modes) see the right column. The plots on the first row report the ST distribution $n_m(\omega)$ from Eq.(2), the plots on the second and third rows display cross-sections of the corresponding distributions in the top row: temporal spectra $n_m(\omega)$ for different mode groups g (2nd row); spatial mode distribution integrated in frequency, $\tilde{n}_m = (2\pi c_0)^{-1} \int n_m(\omega) d\omega$ (3rd row). In (b) the curves refer (from top-to-bottom) to the mode group $g = 1, 3, 6, 10, 16$; while in (e) they refer to the mode group $g = 5, 15, 30, 60, 80, 107$. Remark the significant spectral narrowing in the highest mode group (top curve in (b) and (e)) when the number of modes increases. Parameters are given in the text.

We remark that the first term of the integrand diverges for a vanishing dispersion coefficient, $\kappa = 0$. This reflects

the fact that there is no BE condensation in the pure 2D spatial domain for negative temperatures [120]. Here, thanks to the longitudinal temporal dimension, the photon density ρ converges, which defines a non-vanishing negative critical temperature \tilde{T}_c for inverted BE condensation:

$$\rho = \frac{|\tilde{T}_c|^{5/2}}{2c_0\sqrt{\pi\kappa\beta_0^2}} \left[-\frac{V_0}{\tilde{T}_c} \zeta\left(\frac{3}{2}\right) - \zeta\left(\frac{5}{2}\right) + g_{5/2}\left(e^{\frac{V_0}{\tilde{T}_c}}\right) \right]. \quad (21)$$

For $\tilde{T} > |\tilde{T}_c|$ and $\tilde{\mu} = V_0$, the singularity of the BE distribution is regularized by a macroscopic population of the highest energy level β_{\max} at the frequency $\omega = 0$. The fraction of particle density condensed in the highest energy level $\beta_{\max} = V_0$ at $\omega = 0$ is

$$\frac{\rho_{G0}}{\rho} = 1 - \left(\frac{\tilde{T}_c}{\tilde{T}} \right)^{5/2} \frac{g_{5/2}\left(e^{V_0/\tilde{T}}\right) - \zeta(5/2) - \frac{V_0}{\tilde{T}} \zeta(3/2)}{g_{5/2}\left(e^{V_0/\tilde{T}_c}\right) - \zeta(5/2) - \frac{V_0}{\tilde{T}_c} \zeta(3/2)}. \quad (22)$$

We recall that ρ_{G0} denotes the total population of the G -fold degenerate energy level associated with the eigenvalue β_{\max} (at $\omega = 0$), so that the corresponding population of each individual degenerate mode is reduced by a factor G . According to (22), the condensate vanishes at the negative critical temperature, $\rho_{G0} = 0$ at $\tilde{T} = \tilde{T}_c < 0$, and the condensate fraction increases toward one as the temperature increases to zero, $\rho_{G0}/\rho \rightarrow 1$ as $\tilde{T} \rightarrow 0^-$. As compared to (11), note that the different value 5/2 of the exponent (instead of 3/2) in (22) and the presence of different $g_p(z)$ functions is due to the parabolic waveguide geometry under consideration (the case of a homogeneous step-index waveguide is considered in the Appendix VII).

Using the same argument as in section III B, ρ_{G0} is also the particle density in the highest energy level β_{\max} integrated along the frequency ω , that is ρ_G . This is because the contribution of the density at β_{\max} and $\omega \neq 0$ is negligible in the ST continuum limit. Accordingly, in the thermodynamic limit, the ST condensate given by Eq.(22) coincides with the spatial condensate that populates the highest energy level

$$\rho_{G0}(\tilde{T}) = \rho_G(\tilde{T}). \quad (23)$$

We finally note that, for $\tilde{T} < \tilde{T}_c < 0$, the photon density reads

$$\rho = \frac{|\tilde{T}|^{5/2}}{2c_0\beta_0^2\sqrt{\pi\kappa}} \left[-\frac{V_0}{\tilde{T}} g_{3/2}\left(e^{(\tilde{\mu}-V_0)/\tilde{T}}\right) - g_{5/2}\left(e^{(\tilde{\mu}-V_0)/\tilde{T}}\right) \right. \\ \left. + g_{5/2}\left(e^{\tilde{\mu}/\tilde{T}}\right) \right]. \quad (24)$$

As expected, this expression well recovers Eq.(21) when the critical point is approached, that is in the limit $\tilde{T} \rightarrow \tilde{T}_c^-$ and $\tilde{\mu} \rightarrow V_0^+$.

C. Spectral narrowing by increasing the number of modes

We have seen that 2D spatial condensation tends to evolve into a fully (2+1)D ST condensation by increasing the transverse size of the waveguide. This suggests that also in the negative temperature case, the temporal spectrum of the highest energy level should exhibit significant spectral narrowing as the waveguide becomes wider. We illustrate this property in Fig. 6, which reports the ST equilibrium distribution $n_m(\omega)$ given in Eq.(2) for a parabolic multimode waveguide with $G = 17$ (left column), and $G = 108$ (right column), groups of degenerate modes. Here, we have considered a partially condensed case where $\tilde{T} = -0.4|\tilde{T}_c|$, while the corresponding value of the chemical potential is obtained by solving Eq.(18) for a given value of ρ/S . We considered in Fig. 6 the following parameters: $V_0 = 126\,093\,m^{-1}$, $P = 1\,W$, i.e., $\rho/S = 4.4 \times 10^{16}\,m^{-3}$ or $I = P/S = 3.5 \times 10^6\,W \cdot m^{-2}$. We remark that spectral narrowing in Fig. 6 occurs for the highest mode group at $\beta = \beta_{\max}$. Note that the less pronounced peak around $\omega = 0$ in (b,e) compared to the corresponding plots in Fig. 3 is related to the strong degeneracy of the highest-order mode for the parabolic waveguide under consideration.

V. CONCLUSIONS

In this study, we introduced a theoretical model that permits a general understanding of the ST equilibrium properties of optical waves propagating in multimode waveguides. Our approach led us to predict that ST incoherent light waves exhibit a transition to condensation when the size (i.e., the number of transverse modes) of the waveguide is increased, eventually leading to complete (2+1)D ST condensation in the thermodynamic limit.

In the anomalous dispersion regime of the waveguide, the condensed state is characterized by a macroscopic occupation of the fundamental spatial mode, accompanied by a dramatic spectral narrowing of light carried in the same mode. Conversely, in the normal dispersion regime the ST equilibrium distribution is characterized by negative temperatures, whereby high-order spatial modes are more populated than low-order modes, while the temporal spectrum remains peaked at the fundamental (carrier) frequency. In this way, ST incoherent light exhibits an inverted transition to BE condensation at negative temperatures, which occurs by increasing the temperature above a negative critical value. The condensed state is characterized by a macroscopic population of the highest energy level $\beta = \beta_{\max}$ at the carrier optical frequency (i.e., $\omega = 0$). In addition, we have shown that the ST configuration allows one to discriminate the classical RJ equilibrium from the quantum BE equilibrium: this can be done through the analysis of the spatial mode distribution and temporal spectrum, but also through the trans-

verse spatial near-field intensity distribution, a quantity that can easily be measured in an optical experiment.

Work is in progress to extend the present analysis to nontrivial ST coupling by considering a general model of light propagation that goes beyond the paraxial and slowly-varying-envelope approximations. Along this line, ST thermalization can be investigated by considering temporally incoherent (ASE) sources, which may exploit ST instabilities [100, 101] or supercontinuum generation [63, 103, 105] in multimode fibers. The observation of ST thermalization requires minimizing the detrimental impact of the dissipative Raman effect [142, 143]: as an alternative to optical fibers, other experimental platforms may be considered to suppress this effect, such as optically induced waveguides in atomic vapors [3, 29] photorefractive crystals [122], or gas-filled hollow-core photonic crystal fibers [144].

An important aspect that has not been addressed in this paper involves the nonequilibrium dynamics that drives the field to ST thermal equilibrium. It has recently been shown in Ref.[119] that the temporal degrees of freedom can dramatically accelerate the rate of thermalization to thermal equilibrium. On the other hand, different studies based on wave turbulence theory [56, 66, 73, 89] have revealed that a significant acceleration of the nonequilibrium process of thermalization in multimode fibers is also provided by the structural disorder and the random mode coupling due to refractive index fluctuations introduced by inherent imperfections and environmental perturbations [145–150]. Since the aforementioned studies [56, 66, 73, 89] have been carried out within the framework of purely spatial dynamics, a natural and important extension will be to incorporate structural disorder into the ST wave turbulence theory developed in Ref.[119]. This would allow for a more comprehensive understanding of how disorder influences the nonequilibrium dynamics of ST thermalization in multimode optical systems.

It would also be interesting to extend the present study to investigate the onset of condensation in regimes beyond the weakly nonlinear limit, where linear dispersion effects dominate over the nonlinear Kerr contribution. The stronger nonlinearities in this regime holds the potential to reveal a wealth of new physical phenomena. In this regime, the condensate no longer simply coexists with the uncondensed thermal background, but instead emerges as a distinct phase characterized by remarkable physical behaviors that are absent in the weakly nonlinear case. For instance, it may exhibit superfluidity, allowing for frictionless propagation of Bogoliubov sound waves [8, 9, 11]. Moreover, the dynamics can become highly complex and turbulent, exhibiting phenomena such as the formation and interaction of vortices, i.e., quantum turbulence [151]. The prospect of investigating ST superfluidity, and ST quantum turbulence at positive, or even negative, temperatures within an optical multimode waveguide represents a compelling and largely unexplored frontier, open for future research.

VI. ACKNOWLEDGEMENT

Funding was provided by Agence Nationale de la Recherche (Grants No. ANR-23-CE30-0021, No. ANR-21-ESRE-0040). Calculations were performed using HPC resources from Université Côte d’Azur’s Center Azzura, and DNUM-CCUB (Université de Bourgogne Europe). I.C. acknowledges financial support from the PE0000023-NQSTI project by the Italian Ministry of University and Research, co-funded by the European Union - NextGeneration EU; from Provincia Autonoma di Trento (PAT), partly via the Q@TN initiative. M.F. acknowledges funding from the Italian Ministry of University and Research (MUR) through the Italian Science Fund (FIS2), project SOFT (H53C24001530001). S.W. acknowledges support from the European Innovation Council, project MULTISCOPE (101185664).

VII. APPENDIX

A. Bose-Einstein condensation at negative temperatures in a step-index multimode waveguide

To complete our discussion in Sec. IV, we show that BE condensation at negative temperatures also occurs in step-index multimode waveguides. We consider Eq.(18) in the continuous thermodynamic limit [see (7)], with the DOS $\varrho(\beta) = \varrho_0 = k_0 S / (2\pi)$. The longitudinal photon

density $\rho = \int \frac{d\omega}{2\pi c_0} \int_0^{V_0} d\beta \varrho(\beta) n(\beta, \omega)$ reads

$$\rho = \frac{\varrho_0(-\tilde{T})^{3/2}}{2c_0\sqrt{\pi\kappa}} \left[g_{3/2}(e^{(\tilde{\mu}-V_0)/\tilde{T}}) - g_{3/2}(e^{\tilde{\mu}/\tilde{T}}) \right], \quad (25)$$

where we recall that $\kappa > 0$ and $\tilde{\mu} \geq V_0 = \beta_{\max}$. We remark that $\tilde{\mu} \rightarrow V_0^+$ for a non-vanishing negative critical temperature \tilde{T}_c :

$$\rho = \frac{\varrho_0(-\tilde{T}_c)^{3/2}}{2c_0\sqrt{\pi\kappa}} \left[\zeta(3/2) - g_{3/2}(e^{V_0/\tilde{T}_c}) \right], \quad (26)$$

To provide a complementary perspective to the previous parabolic waveguide analysis in Sec. IV (where the highest energy level was degenerate), here we consider a step-index waveguide with a non-degenerate highest energy level. By increasing the negative temperature above \tilde{T}_c , the photon gas undergoes a transition to BE condensation characterized by a macroscopic population of the highest mode M with propagation constant $\beta_{\max} = V_0$ at $\omega = 0$:

$$\frac{\rho_{M0}}{\rho} = 1 - \left(\frac{\tilde{T}}{\tilde{T}_c} \right)^{3/2} \frac{\zeta(3/2) - g_{3/2}(e^{V_0/\tilde{T}})}{\zeta(3/2) - g_{3/2}(e^{V_0/\tilde{T}_c})}. \quad (27)$$

The condensate vanishes at and below the negative critical temperature, $\rho_{M0}/\rho = 0$ at $\tilde{T} \leq \tilde{T}_c < 0$, and increases to one as the temperature increases to zero, $\rho_{M0}/\rho \rightarrow 1$ as $\tilde{T} \rightarrow 0^-$.

[1] I. Carusotto, C. Ciuti, Quantum fluids of light, *Rev. Modern Phys.* **85**, 299 (2013).

[2] J. Bloch, I. Carusotto, M. Wouters, Nonequilibrium Bose-Einstein condensation in photonic systems, *Nature Phys. Rev.* **4** (2022) 470.

[3] Q. Glorieux, T. Aladjidi, P.D. Lett, R. Kaiser, Hot atomic vapors for nonlinear and quantum optics, *New J. Phys.* **25**, 051201 (2023).

[4] Q. Glorieux, C. Piekarski, Q. Schibler, T. Aladjidi, M. Baker-Rasooli, Paraxial fluids of light, *Advances In Atomic, Molecular, and Optical Physics* **74**, 157-241 (2025).

[5] L.G. Wright, F.O. Wu, D.N. Christodoulides, F.W. Wise, Physics of highly multimode nonlinear optical systems, *Nature Physics* **18**, 1018 (2022).

[6] M. Ferraro, F. Mangini, M. Zitelli, S. Wabnitz, On spatial beam self-cleaning from the perspective of optical wave thermalization in multimode graded-index fibers, *Advances in Physics: X* **8**, 2228018 (2023).

[7] P-E. Larré and I. Carusotto, Propagation of a quantum fluid of light in a cavityless nonlinear optical medium: General theory and response to quantum quenches, *Phys. Rev. A* **92**, 043802 (2015).

[8] Q. Fontaine, T. Bienaimé, S. Pigeon, E. Giacobino, A. Bramati, and Q. Glorieux, Observation of the Bogoliubov Dispersion in a Fluid of Light, *Phys. Rev. Lett.* **121**, 183604 (2018).

[9] C. Michel, O. Boughdad, M. Albert, P.-E. Larré, and M. Bellec, Superfluid motion and drag-force cancellation in a fluid of light, *Nature Communications* **9**, 2108 (2018).

[10] G. Situ, J.W. Fleischer, Dynamics of the Berezinskii-Kosterlitz-Thouless transition in a photon fluid, *Nature Photonics* **14**, 517 (2020).

[11] A. Eloy, O. Boughdad, M. Albert, P.-E. Larré, F. Mortessagne, M. Bellec, and C. Michel, Experimental observation of turbulent coherent structures in a superfluid of light, *Europhysics Letters* **134**, 26001 (2021).

[12] M. Baker-Rasooli, W. Liu, T. Aladjidi, A. Bramati, Q. Glorieux, Turbulent dynamics in a two-dimensional paraxial fluid of light, *Phys. Rev. A* **108**, 063512 (2023).

[13] T. Congy, P. Azam, R. Kaiser, and N. Pavloff, Topological Constraints on the Dynamics of Vortex Formation in a Two-Dimensional Quantum Fluid, *Phys. Rev. Lett.* **132**, 033804 (2024).

[14] R. Panico, G. Ciliberto, G.I. Martone, T. Congy, D. Ballarini, A.S. Lanotte and N. Pavloff, Topological pathways to two-dimensional quantum turbulence, *Phys. Rev. Res.* **7**, L022063 (2025).

[15] C. Piekarski, N. Cheroret, T. Aladjidi, Q. Glorieux, Spin and Density Modes in a Binary Fluid of Light, *Phys. Rev. Lett.* **134**, 223403 (2025).

[16] G.I. Martone, T. Bienaimé, N. Cheroret, Spin-orbit-

coupled fluids of light in bulk nonlinear media, *Phys. Rev. A* **104**, 013510 (2021).

[17] G.I. Martone, N. Cherroret, Time Translation Symmetry Breaking in an Isolated Spin-Orbit-Coupled Fluid of Light, *Phys. Rev. Lett.* **131**, 013803 (2023).

[18] R. Bekenstein, R. Schley, M. Mutzafi, C. Rotschild, and M. Segev, Optical simulations of gravitational effects in the Newton-Schrödinger system, *Nat. Phys.* **11**, 872 (2015).

[19] T. Roger, C. Maitland, K. Wilson, N. Westerberg, D. Vocke, E. M. Wright, and D. Faccio, Optical analogues of the Newton-Schrödinger equation and boson star evolution, *Nat. Commun.* **7**, 13492 (2016).

[20] F. Marino, Massive phonons and gravitational dynamics in a photon-fluid model, *Phys. Rev. A* **100**, 063825 (2019).

[21] M.C. Braidotti, R. Prizia, C. Maitland, F. Marino, A. Prain, I. Starshynov, N. Westerberg, E.M. Wright, and D. Faccio, Measurement of Penrose superradiance in a photon superfluid, *Phys. Rev. Lett.* **128**, 013901 (2022).

[22] G. Marcucci and C. Conti, Simulating general relativity and non-commutative geometry by non-paraxial quantum fluids, *New Journal of Physics* **21**, 123038 (2019).

[23] S.L. Braunstein, M. Faizal, L.M. Krauss, F. Marino, N.A. Shah, Analogue simulations of quantum gravity with fluids, *Nature Reviews Physics* **5**, 612 (2023).

[24] T.D. Ferreira, V. Rocha, D. Silva, A. Guerreiro, N.A. Silva, Towards the experimental observation of turbulent regimes and the associated energy cascades with paraxial fluids of light, *New Journal of Physics* **24**, 113050 (2022).

[25] M. Baker-Rasooli, W. Liu, T. Aladjidi, A. Bramati, Q. Glorieux, Turbulent dynamics in a two-dimensional paraxial fluid of light, *Phys. Rev. A* **108**, 063512 (2023).

[26] J. Berges, S. Borsanyi, and C. Wetterich, Prethermalization, *Phys. Rev. Lett.* **93**, 142002 (2004).

[27] P.-E. Larré, I. Carusotto, Prethermalization in a quenched one-dimensional quantum fluid of light, Intrinsic limits to the coherent propagation of a light beam in a nonlinear optical fiber, *The European Physical Journal D* **70**, 45 (2016).

[28] M. Abuzarli, N. Cherroret, T. Bienaimé, Q. Glorieux, Nonequilibrium Prethermal States in a Two-Dimensional Photon Fluid, *Phys. Rev. Lett.* **129**, 100602 (2022).

[29] J. Steinhauer, M. Abuzarli, T. Aladjidi, T. Bienaimé, C. Piekarski, W. Liu, E. Giacobino, A. Bramati, Q. Glorieux, Analogue cosmological particle creation in an ultracold quantum fluid of light, *Nature Communications* **13**, 2890 (2022).

[30] A. Chiocchetta, P.E. Larré, I. Carusotto, Thermalization and Bose-Einstein condensation of quantum light in bulk nonlinear media, *Europhysics Letters* **115**, 24002 (2016).

[31] M.J. Davis, S.A. Morgan, K. Burnett, Simulations of Bose Fields at Finite Temperature, *Phys. Rev. Lett.* **87**, 160402 (2001).

[32] C. Connaughton, C. Josserand, A. Picozzi, Y. Pomeau, S. Rica, Condensation of classical nonlinear waves, *Phys. Rev. Lett.* **95**, 263901 (2005).

[33] P.B. Blakie, A.S. Bradley, M.J. Davis, R.J. Ballagh, C.W. Gardiner, Dynamics and statistical mechanics of ultra-cold Bose gases using c-field techniques, *Advance in Physics* **57**, 363-455 (2008).

[34] G. Krstulovic, M. Brachet, Energy cascade with small-scale thermalization, counterflow metastability, and anomalous velocity of vortex rings in Fourier truncated Gross-Pitaevskii equation, *Phys. Rev. E* **83**, 066311 (2011).

[35] S. Nazarenko, *Wave Turbulence* (Springer, Lectures Notes in Physics, 2011).

[36] A. Picozzi, J. Garnier, T. Hansson, P. Suret, S. Randoux, G. Millot, and D. N. Christodoulides, Optical wave turbulence: Toward a unified nonequilibrium thermodynamic formulation of statistical nonlinear optics, *Phys. Rep.* **542**, 1 (2014).

[37] J. Klaers, J. Schmitt, F. Vewinger, M. Weitz, Bose-Einstein condensation of photons in an optical microcavity, *Nature* **468**, 545 (2010).

[38] J. Klaers, F. Vewinger, M. Weitz, Thermalization of a two-dimensional photonic gas in a ‘white-wall’ photon box, *Nature Physics* **6**, 512 (2010).

[39] T. Damm, J. Schmitt, Qi Liang, D. Dung, F. Vewinger, M. Weitz, J. Klaers, Calorimetry of a Bose-Einstein-condensed photon gas, *Nature Communications* **7**, 11340 (2016).

[40] B.T. Walker, L.C. Flatten, H.J. Hesten, F. Mintert, D. Hunger, A.A.P. Trichet, J.M. Smith, R.A. Nyman, Driven-dissipative non-equilibrium Bose-Einstein condensation of less than ten photons, *Nature Physics* **14**, 1173 (2018).

[41] R. Weill, A. Bekker, B. Levit, B. Fischer, Bose-Einstein condensation of photons in an erbium-ytterbium codoped fiber cavity, *Nature Communications* **10**, 1-6 (2019).

[42] R. Weill, A. Bekker, B. Levit, and B. Fischer, Bose-Einstein condensation of photons in a long fiber cavity, *Optics Express* **29**, 27807 (2021).

[43] S. Barland, P. Azam, G.L. Lippi, R.A. Nyman, and R. Kaiser, Photon thermalization and a condensation phase transition in an electrically pumped semiconductor microresonator, *Optics Express* **29**, 8368 (2021).

[44] C. Conti, M. Leonetti, A. Fratalocchi, L. Angelani, G. Ruocco, Condensation in Disordered Lasers: Theory, 3d+1 Simulations, and Experiments, *Phys. Rev. Lett.* **101**, 143901 (2008).

[45] C. Michel, M. Haelterman, P. Suret, S. Randoux, R. Kaiser, and A. Picozzi, Thermalization and condensation in an incoherently pumped passive optical cavity, *Phys. Rev. A* **84**, 033848 (2011).

[46] R. Weill, B. Fischer, and O. Gat, Light-Mode Condensation in Actively-Mode-Locked Lasers, *Phys. Rev. Lett.* **104**, 173901 (2010).

[47] N. G. Berloff, J. Keeling, Universality in modelling nonequilibrium polariton condensates, in *Physics of Quantum Fluids*, edited by A. Bramati and M. Modugno, Springer Series in Solid-State Sciences Vol. 177 (Springer, Berlin, 2013).

[48] E. Turitsyna, G. Falkovich, A. El-Taher, X. Shu, P. Harper, S. Turitsyn, Optical turbulence and spectral condensate in long fibre lasers, *Proc. R. Soc. London Ser. A* **468**, 2145 (2012).

[49] D. Churkin, I. Kolokolov, E. Podivilov, I. Vatnik, S. Vergeles, I. Terekhov, V. Lebedev, G. Falkovich, M. Nikulin, S. Babin, S. Turitsyn, Wave kinetics of a random fibre laser, *Nature Communications* **2**, 6214 (2015).

[50] J. Huang, C. Liu, Y. Zhu, S. Masala, E. Alarousu, Y. Han, and A. Fratalocchi, Harnessing structural darkness

in the visible and infrared wavelengths for a new source of light, *Nature Nanotech.* **11**, 60 (2015).

[51] M. Conforti, A. Mussot, J. Fatome, A. Picozzi, S. Pitois, C. Finot, M. Haelterman, B. Kibler, C. Michel, G. Millot, Turbulent dynamics of an incoherently pumped passive optical fiber cavity: Quasisolitons, dispersive waves, and extreme events, *Phys. Rev. A* **91**, 023823 (2015).

[52] P. Aschieri, J. Garnier, C. Michel, V. Doya, and A. Picozzi, Condensation and thermalization of classical optical waves in a waveguide, *Phys. Rev. A* **83**, 033838 (2011).

[53] V.E. Zakharov, V.S. L'vov, G. Falkovich, *Kolmogorov Spectra of Turbulence I* (Springer, Berlin, 1992).

[54] A.C. Newell, B. Rumpf, Wave Turbulence, *Annu. Rev. Fluid Mech.* **43**, 59 (2011).

[55] S.K. Turitsyn, S.A. Babin, E.G. Turitsyna, G. E. Falkovich, E. Podivilov, D. Churkin, Optical Wave Turbulence, in *Advances in Wave Turbulence*, World Scientific Series on Nonlinear Science Series A, Vol. 83, edited by V.I. Shrira and S. Nazarenko (World Scientific, Singapore, 2013).

[56] A. Fusaro, J. Garnier, K. Krupa, G. Millot, A. Picozzi, Dramatic acceleration of wave condensation mediated by disorder in multimode fibers, *Phys. Rev. Lett.* **122**, 123902 (2019).

[57] K. Baudin, A. Fusaro, K. Krupa, J. Garnier, S. Rica, G. Millot, A. Picozzi, Classical Rayleigh-Jeans condensation of light waves: Observation and thermodynamic characterization, *Phys. Rev. Lett.* **125**, 244101 (2020).

[58] K. Baudin, A. Fusaro, J. Garnier, N. Berti, K. Krupa, I. Carusotto, S. Rica, G. Millot, A. Picozzi, Energy and wave-action flows underlying Rayleigh-Jeans thermalization of optical waves propagating in a multimode fiber, *Europhys. Lett.* **134**, 14001 (2021).

[59] H. Pourbeyram, P. Sidorenko, F. Wu, L. Wright, D. Christodoulides, F. Wise, Direct observations of thermalization to a Rayleigh-Jeans distribution in multimode optical fibres, *Nature Physics* **18**, 685 (2022).

[60] F. Mangini, M. Gervaziev, M. Ferraro, D. S. Kharenko, M. Zitelli, Y. Sun, V. Couderc, E.V. Podivilov, S.A. Babin, and S. Wabnitz, Statistical mechanics of beam self-cleaning in GRIN multimode optical fibers, *Opt. Exp.* **30**, 10850 (2022).

[61] E.V. Podivilov, F. Mangini, O.S. Sidelnikov, M. Ferraro, M. Gervaziev, D.S. Kharenko, M. Zitelli, M.P. Fedoruk, S.A. Babin, S. Wabnitz, Thermalization of orbital angular momentum beams in multimode optical fibers, *Phys. Rev. Lett.* **128**, 243901 (2022).

[62] F. Mangini, M. Ferraro, A. Tonello, V. Couderc, and S. Wabnitz, High-temperature wave thermalization spoils beam self-cleaning in nonlinear multimode GRIN fibers, *Opt. Lett.* **48**, 4741 (2023).

[63] L.G. Wright, Z. Liu, D.A. Nolan, M.-J. Li, D.N. Christodoulides, F.W. Wise, Self-organized instability in graded-index multimode fibres, *Nature Photonics* **10**, 771 (2016).

[64] K. Krupa, A. Tonello, B.M. Shalaby, M. Fabert, A. Barthélémy, G. Millot, S. Wabnitz, V. Couderc, Spatial beam self-cleaning in multimode fibres, *Nature Photonics* **11**, 237 (2017).

[65] E. Podivilov, D. Kharenko, V. Gonta, K. Krupa, O.S. Sidelnikov, S. Turitsyn, M.P. Fedoruk, S.A. Babin, S. Wabnitz, Hydrodynamic 2D turbulence and spatial beam condensation in multimode optical fibers, *Phys. Rev. Lett.* **122**, 103902 (2019).

[66] J. Garnier, A. Fusaro, K. Baudin, C. Michel, K. Krupa, G. Millot, A. Picozzi, Wave condensation with weak disorder versus beam self-cleaning in multimode fibers, *Phys. Rev. A* **100**, 053835 (2019).

[67] F.O. Wu, A.U. Hassan, D.N. Christodoulides, Thermodynamic theory of highly multimoded nonlinear optical systems, *Nature Photonics* **13**, 776 (2019).

[68] O. S. Sidelnikov, E. V. Podivilov, M. P. Fedoruk, and S. Wabnitz, Random mode coupling assists Kerr beam selfcleaning in a graded-index multimode optical fiber, *Opt. Fiber Technol.* **53**, 101994 (2019).

[69] M. Parto, F. O. Wu, P. S. Jung, K. Makris, and D. N. Christodoulides, Thermodynamic conditions governing the optical temperature and chemical potential in nonlinear highly multimoded photonic systems, *Opt. Lett.* **44**, 3936 (2019).

[70] K. G. Makris, F. Wu, P. S. Jung, and D. N. Christodoulides, Statistical mechanics of weakly nonlinear optical multimode gases, *Opt. Lett.* **45**, 1651 (2020).

[71] F.O. Wu, Q. Zhong, H. Ren, P.S. Jung, K.G. Makris, D.N. Christodoulides, Thermalization of Light's orbital angular momentum in nonlinear multimode waveguide systems, *Phys. Rev. Lett.* **128**, 123901 (2022).

[72] M. Ferraro, F. Mangini, M. Zitelli, S. Wabnitz, On spatial beam self-cleaning from the perspective of optical wave thermalization in multimode graded-index fibers, *Advances in Physics: X* **8**, 2228018 (2023).

[73] M. Ferraro, K. Baudin, M. Gervaziev, A. Fusaro, A. Picozzi, J. Garnier, G. Millot, D. Kharenko, E. Podivilov, S. Babin, F. Mangini, S. Wabnitz, Wave turbulence, thermalization and multimode locking in optical fibers *Physica D* **481**, 134758 (2025).

[74] M. Zitelli, V. Couderc, M. Ferraro, F. Mangini, P. Parra-Rivas, Y. Sun, S. Wabnitz, Spatiotemporal mode decomposition of ultrashort pulses in linear and nonlinear graded-index multimode fibers, *Photon. Res.* **11**, 750 (2023).

[75] M. Zitelli, F. Mangini, S. Wabnitz, Statistics of modal condensation in nonlinear multimode fibers, *Nature Communications* **15**, 1149 (2024).

[76] J. Zhang, J. Fan, C. Mei, G. Steinmeyer, M. Hu, Bose-Einstein condensation of an optical thermodynamic system into a solitonic state, arXiv:2405.13716

[77] A.Y. Ramos, C. Shi, L.J. Fernandez-Alcazar, D.N. Christodoulides, T. Kottos, Theory of localization-hindered thermalization in nonlinear multimode photonics, *Communications Physics* **6**, 189 (2023).

[78] L.G. Wright, F.O. Wu, D.N. Christodoulides, F.W. Wise, Physics of highly multimode nonlinear optical systems, *Nature Physics* **18**, 1018 (2022).

[79] A. Ramos, L. Fernández-Alcázar, T. Kottos, B. Shapiro, Optical Phase Transitions in Photonic Networks: a Spin-System Formulation, *Phys. Rev. X* **10**, 031024 (2020).

[80] H. Ren, G.G. Pyrialakos, F.O. Wu, P.S. Jung, N.K. Efremidis, M. Khajavikhan, D.N. Christodoulides, Nature of optical thermodynamic pressure exerted in highly multimoded nonlinear systems, *Phys. Rev. Lett.* **131**, 193802 (2023).

[81] N.K. Efremidis, D.N. Christodoulides, Statistical mechanics and pressure of composite multimoded weakly nonlinear optical systems, *Opt. Lett.* **49**, 2777 (2024).

[82] G. Yang, D. Bongiovanni, D. Song, R. Morandotti, Z.

Chen, N.K. Efremidis, Thermalization dynamics in photonic lattices of different geometries, *APL Photonics* **9**, 066115 (2024).

[83] H. Ren, G.G. Pyrialakos, Q. Zhong, F.O. Wu, M. Khajavikhan, D.N. Christodoulides, Photon–photon chemical thermodynamics of frequency conversion processes in highly multimode systems, *Light: Science & Applications* (2025) 14:188.

[84] K. Baudin, J. Garnier, A. Fusaro, N. Berti, C. Michel, K. Krupa, G. Millot, A. Picozzi, Observation of light thermalization to negative temperature Rayleigh–Jeans equilibrium states in multimode optical fibers, *Phys. Rev. Lett.* **130**, 063801 (2023).

[85] A.L. Muniz, F. Wu, P. Jung, M. Khajavikhan, D. Christodoulides, U. Peschel, Observation of photon–photon thermodynamic processes under negative optical temperature conditions, *Science* **379**, 1019 (2023).

[86] M. Ferraro, F. Mangini, K. Stefánska, W.A. Gemedu, F. Frezza, V. Couderc, M. Gervaziev, D. Kharenko, S. Babin, and S. Wabnitz, Negative absolute temperature attractor in a dense photon gas, arXiv:2505.21163

[87] M. Ferraro, F. Mangini, F.O. Wu, M. Zitelli, D.N. Christodoulides, S. Wabnitz, Calorimetry of photon gases in nonlinear multimode optical fibers, *Phys. Rev. X* **14**, 021020 (2024).

[88] M.S. Kirsch, G.G. Pyrialakos, R. Altenkirch, M.A. Selim, J. Beck, T.A.W. Wolterink, H. Ren, P.S. Jung, M. Khajavikhan, A. Szameit, M. Heinrich, D.N. Christodoulides, Observation of Joule–Thomson photon–gas expansion, *Nat. Phys.* **21**, 214 (2025)

[89] N. Berti, K. Baudin, A. Fusaro, G. Millot, A. Picozzi, J. Garnier, Interplay of thermalization and strong disorder: Wave turbulence theory, numerical simulations, and experiments in multimode optical fibers, *Phys. Rev. Lett.* **129**, 063901 (2022).

[90] M. Lian, Y. Geng, Y.-J. Chen, Y. Chen, J.-T. Lü, Coupled Thermal and Power Transport of Optical Waveguide Arrays: Photonic Wiedemann–Franz Law and Rectification Effect, *Phys. Rev. Lett.* **133**, 116303 (2024).

[91] A. Kurnosov, L.J. Fernández-Alcázar, A. Ramos, B. Shapiro, T. Kottos, Optical Kinetic Theory of Nonlinear Multimode Photonic Networks, *Phys. Rev. Lett.* **132**, 193802 (2024).

[92] Y. Liu, J. Lu, Z. Xiong, F.O. Wu, D. Christodoulides, Y. Chen, J.H. Jiang, Nonequilibrium transport and the fluctuation theorem in the thermodynamic behaviors of nonlinear photonic systems, *Phys. Rev. Res.* **7**, 013084 (2025).

[93] G. Yang, J. Wang, Y. Chen, L. Song, S. Xia, D. Song, Z. Chen, N.K. Efremidis, Unveiling prethermalization and thermal processes through the simplest one-dimensional topological model, arXiv:2507.04101

[94] Y. Castin, R. Dum, E. Mandonnet, A. Minguzzi and I. Carusotto, Coherence properties of a continuous atom laser, *Journal of Modern Optics* **47**, 2671 (2000).

[95] E. Mandonnet, A. Minguzzi, R. Dum, I. Carusotto, Y. Castin, J. Dalibard, Evaporative cooling of an atomic beam, *Eur. Phys. J. D* **10**, 9 (2000).

[96] T. Lahaye, Z. Wang, G. Reinaudi, S.P. Rath, J. Dalibard, D. Guéry-Odelin, Evaporative cooling of a guided rubidium atomic beam, *Phys. Rev. A* **72**, 033411 (2005).

[97] S.E. Olson, R.R. Mhaskar, G. Raithel, Continuous propagation and energy filtering of a cold atomic beam in a long high-gradient magnetic atom guide, *Phys. Rev. A* **73**, 033622 (2006).

[98] C.-C. Chen, S. Bennetts, R.G. Escudero, B. Pasquiou, F. Schreck, Continuous guided strontium beam with high phase-space density, *Phys. Rev. Appl.* **12**, 044014 (2019);

[99] G. Agrawal, *Nonlinear Fiber Optics* (Academic, New York, 6th ed., 2019).

[100] L.G. Wright, S. Wabnitz, D. Christodoulides, F. Wise, Ultrabroadband dispersive radiation by spatiotemporal oscillation of multimode waves, *Phys. Rev. Lett.* **115**, 223902 (2015).

[101] K. Krupa, A. Tonello, A. Barthélémy, V. Couderc, B.M. Shalaby, A. Bendahmane, G. Millot, S. Wabnitz, Observation of geometric parametric instability induced by the periodic spatial self-imaging of multimode waves, *Phys. Rev. Lett.* **116**, 183901 (2016).

[102] C. Mas Arabí, A. Kudlinski, A. Mussot, M. Conforti, Geometric parametric instability in periodically modulated graded-index multimode fibers, *Phys. Rev. A* **97**, 023803 (2018).

[103] K. Krupa, C. Louot, V. Couderc, M. Fabert, R. Guenard, B. M. Shalaby, A. Tonello, D. Pagnoux, P. Leproux, A. Bendahmane, R. Dupiol, G. Millot, and S. Wabnitz, Spatiotemporal characterization of supercontinuum extending from the visible to the mid-infrared in a multimode graded-index optical fiber, *Opt. Lett.* **41**, 5785 (2016).

[104] B. Kibler, P. Béjot, Discretized Conical Waves in Multimode Optical Fibers, *Phys. Rev. Lett.* **126**, 023902 (2021).

[105] Z. Eslami, L. Salmela, A. Filipkowski, D. Pysz, M. Klimczak, R. Buczynski, J.M. Dudley, G. Genty, Two octave supercontinuum generation in a non-silica graded-index multimode fiber, *Nature Comm.* **13**, 2126 (2022).

[106] Y. Leventoux, G. Granger, K. Krupa, A. Tonello, G. Millot, M. Ferraro, F. Mangini, M. Zitelli, S. Wabnitz, S. Février, and V. Couderc, 3D time-domain beam mapping for studying nonlinear dynamics in multimode optical fibers, *Opt. Lett.*, **46**, 66 (2021).

[107] K. Stefánska, P. Béjot, K. Tarnowski, B. Kibler Experimental Observation of the Spontaneous Emission of a Space–Time Wavepacket in a Multimode Optical Fiber, *ACS Photonics* **10**, 727 (2023).

[108] S.A. Babin, D.V. Churkin, A.E. Ismagulov, S.I. Kablukov, E.V. Podivilov, Four-wave-mixing-induced turbulent spectral broadening in a long Raman fiber laser, *J. Opt. Soc. Am. B* **24**, 1729–1738 (2007).

[109] B. Barviau, B. Kibler, A. Kudlinski, A. Mussot, G. Millot, A. Picozzi, Experimental signature of optical wave thermalization through supercontinuum generation in photonic crystal fiber, *Optics Express* **17**, 7392 (2009).

[110] S. Pitois, S. Lagrange, H.R. Jauslin, A. Picozzi, Velocity locking of incoherent nonlinear wave packets, *Phys. Rev. Lett.* **97**, 033902 (2006).

[111] P. Suret, S. Randoux, H. Jauslin, A. Picozzi, Anomalous thermalization of nonlinear wave systems, *Phys. Rev. Lett.* **104** (2010) 054101.

[112] P. Suret, A. Picozzi, S. Randoux, Wave turbulence in integrable systems: nonlinear propagation of incoherent optical waves in single-mode fibers, *Opt. Express* **19**, 17852 (2011).

[113] S. K. Turitsyn, S. A. Babin, E. G. Turitsyna, G. E. Falkovich, E. Podivilov, D. Churkin, Optical Wave Turbulence, in *Advances in Wave Turbulence* (World Sci-

entific, Singapore, 2013).

[114] D. Churkin, I. Kolokolov, E. Podivilov, I. Vatnik, S. Vergeles, I. Terekhov, V. Lebedev, G. Falkovich, M. Nikulin, S. Babin, S. Turitsyn, Wave kinetics of a random fibre laser, *Nature Communications* **2**, 6214 (2015).

[115] K. Krupa, A. Tonello, V. Couderc, A. Barthélémy, G. Millot, D. Modotto, S. Wabnitz, Spatiotemporal light-beam compression from nonlinear mode coupling, *Phys. Rev. A* **97**, 043836 (2018).

[116] M. Labaz and P. Sidorenko, Spatial-spectral complexity in Kerr beam self-cleaning, *Opt. Lett.* **49**, 2902 (2024).

[117] J. Li, J. Ruelle, P. Ryczkowski, J.M. Dudley; G. Genty, Real-Time Measurements of Beam Self-Cleaning Dynamics, CLEO/Europe EQEC conference (2025), DOI: 10.1109/CLEO-Europe-EQEC65582.2025.11109609

[118] A. Picozzi, Towards a nonequilibrium thermodynamic description of incoherent nonlinear optics, *Optics Express* **15**, 9063 (2007).

[119] L. Zanaglia, J. Garnier, I. Carusotto, V. Doya, C. Michel, A. Picozzi, Spatio-temporal thermalization and adiabatic cooling of guided light waves, arXiv:2506.23536v1

[120] L. Zanaglia, J. Garnier, S. Rica, R. Kaiser, S. Wabnitz, C. Michel, V. Doya, and A. Picozzi, Bridging Rayleigh-Jeans and Bose-Einstein condensation of a guided fluid of light with positive and negative temperatures, *Phys. Rev. A* **110**, 063530 (2024).

[121] For a circular step-index waveguide of radius R , $\beta_m = x_{l,s}^2/(2k_0 R^2)$, where $m = (l, s)$ labels the two integers that specify a mode, with $x_{l,s}$ the s -th zero of the Bessel function of the first kind $J_l(x)$, and k_0 the light wave-number. For a parabolic (GRIN) multimode waveguide, $\beta_m = \beta_0(m_x + m_y + 1)$, where $m = (m_x, m_y)$ labels the two integers that specify a mode, and β_0 is the fundamental mode eigenvalue.

[122] C. Denz, M. Schwab, C. Weilnau, *Transverse-Pattern Formation in Photorefractive Optics* (Springer-Verlag, Berlin, 2003).

[123] M. Abarkan, J. P. Salvestrini, M. D. Fontana and M. Cuniot-Ponsard, Frequency and wavelength dependences of the electro-optic coefficients in SBN:60 single crystal, *Appl. Phys. B* **91**, 489-492 (2008).

[124] M. Abuzarli, Out of equilibrium dynamics in a paraxial fluid of light, PhD Thesis, Sorbonne University, 2022.

[125] The dispersion parameter can be rescaled in the equilibrium distribution by means of the change of variables: $\hat{\beta} = \beta/|\kappa|$, $\hat{T} = \tilde{T}/|\kappa|$, $\hat{\mu} = \tilde{\mu}/|\kappa|$. The corresponding rescaled density of states is given by $\hat{\varrho}(\hat{\beta}) = \varrho(\beta)|\kappa|$, the diffraction parameter $\hat{\alpha}_\perp = \alpha_\perp/|\kappa|$ and the potential depth $\hat{V}_0 = V_0/|\kappa|$.

[126] L. Pitaevskii and S. Stringari, *Bose-Einstein Condensation and Superfluidity* (Oxford University Press) 2016.

[127] The optical energy density can be defined by $\epsilon = \sum_m \int \frac{d\omega}{2\pi} \tilde{\beta}_m(\omega) n_m(\omega)$, whose integral diverges when the RJ equilibrium distribution $n_m^{RJ}(\omega)$ is considered.

[128] M. Gervaziev, I. Zhdanov, D. Kharenko, V. Gonta, V. Volosi, E. Podivilov, S. Babin, and S. Wabnitz, Mode decomposition of multimode optical fiber beams by phase-only spatial light modulator, *Laser Physics Letters* **18**, 015101 (2020).

[129] L. Onsager, Statistical hydrodynamics, *Il Nuovo Cimento* (1943-1954) **6**, 279 (1949).

[130] N.F. Ramsey, Thermodynamics and statistical mechanics at negative absolute temperatures, *Physical Review* **103**, 20 (1956).

[131] M. Baldovin, S. Iubini, R. Livi, and A. Vulpiani, Statistical mechanics of systems with negative temperature, *Physics Reports* **923**, 1 (2021).

[132] D. Frenkel and P.B. Warren, Gibbs, Boltzmann, and negative temperatures, *American Journal of Physics* **83**, 163 (2015).

[133] P. Buonsante, R. Franzosi, and A. Smerzi, On the dispute between Boltzmann and Gibbs entropy, *Annals of Physics* **375**, 414 (2016).

[134] A. Puglisi, A. Sarracino, and A. Vulpiani, Temperature in and out of equilibrium: A review of concepts, tools and attempts, *Physics Reports* **709**, 1 (2017).

[135] L. Cerino, A. Puglisi, and A. Vulpiani, A consistent description of fluctuations requires negative temperatures, *Journal of Statistical Mechanics: Theory and Experiment*, P12002 (2015).

[136] M. Onorato, G. Dematteis, D. Proment, A. Pezzi, M. Ballarin, and L. Rondoni, Equilibrium and nonequilibrium description of negative temperature states in a one-dimensional lattice using a wave kinetic approach, *Phys. Rev. E* **105**, 014206 (2022).

[137] J. Skipp, S. Nazarenko, Equilibria and condensates in Rossby and drift wave turbulence, *J. Phys. A: Math. Theor.* **55**, 015701 (2022).

[138] E. M. Purcell and R. V. Pound, A nuclear spin system at negative temperature, *Physical Review* **81**, 279 (1951).

[139] S. Braun, J. P. Ronzheimer, M. Schreiber, S. S. Hodgman, T. Rom, I. Bloch, and U. Schneider, Negative absolute temperature for motional degrees of freedom, *Science* **339**, 52 (2013).

[140] G. Gauthier, M. T. Reeves, X. Yu, A. S. Bradley, M.A. Baker, T.A. Bell, H. Rubinsztein-Dunlop, M.J. Davis, T.W. Neely, Giant vortex clusters in a two-dimensional quantum fluid, *Science* **364**, 1264 (2019).

[141] S.P. Johnstone, A.J. Groszek, P.T. Starkey, C.J. Billington, T.P. Simula, K. Helmerson, Evolution of large-scale flow from turbulence in a two-dimensional superfluid, *Science* **364**, 1267 (2019).

[142] A. Picozzi, S. Pitois, G. Millot, Spectral incoherent solitons: A localized soliton behavior in frequency space, *Phys. Rev. Lett.* **101**, 093901 (2008).

[143] K. Baudin, J. Garnier, A. Fusaro, N. Berti, G. Millot, A. Picozzi, Weak Langmuir turbulence in disordered multimode optical fibers, *Phys. Rev. A* **105**, 013528 (2022).

[144] P. S. J. Russell, P. Hölzer, W. Chang, A. Abdolvand, J. C. Travers, Hollow-core photonic crystal fibres for gas-based nonlinear optics, *Nature Photonics* **8**, 278 (2014).

[145] A. Mecozzi, C. Antonelli, M. Shtaif, Nonlinear propagation in multimode fibers in the strong coupling regime, *Opt. Express* **20**, 11673 (2012).

[146] A. Mecozzi, C. Antonelli, M. Shtaif, Coupled manakov equations in multimode fibers with strongly coupled groups of modes, *Opt. Express* **20**, 23436 (2012).

[147] S. Mumtaz, R.J. Essiambre, G.P. Agrawal, Nonlinear propagation in multimode and multicore fibers: Generalization of the manakov equations, *J. Lightw. Technol.* **31**, 398 (2013).

[148] Y. Xiao, R.-J. Essiambre, M. Desgroseilliers, A.M. Tulino, R. Ryf, S. Mumtaz, G.P. Agrawal, Theory of intermodal four-wave mixing with random linear mode coupling in few-mode fibers, *Opt. Express* **22**, 32039 (2014).

- [149] D. Psaltis, C. Moser, Imaging with multimode fibers, *Opt. and Photon. News* **27**, 24 (2016).
- [150] P. Caramazza, O. Moran, R. Murray-Smith, D. Faccio, Transmission of natural scene images through a multi-mode fibre, *Nature Commun.* **10**, 2029 (2019).
- [151] M.C. Tsatsos, P.E.S. Tavares, A. Cidrim, A.R. Fritsch, M.A. Caracanhas, F.E.A. dos Santos, C.F. Barenghi, and V.S. Bagnato, Quantum turbulence in trapped atomic Bose-Einstein condensates, *Phys. Rep.* **622**, 1 (2016).